

A False Vacuum Skyrme Model for Nuclear Matter

L. A. Ferreira^{†,1} and L. R. Livramento^{†,*,2}

[†]Instituto de Física de São Carlos; IFSC/USP;
Universidade de São Paulo, USP
Caixa Postal 369, CEP 13560-970, São Carlos-SP, Brazil

*BLTP, JINR, Dubna 141980, Moscow Region, Russia

Abstract

The low energy regime of Quantum Chromodynamics (QCD) presents enormous challenges due to its large coupling. Effective field theories, like the Skyrme model, are useful approaches to study properties of strong interaction at hadronic scales. We propose a Skyrme-type model with a self-dual sector and that treats the density of the baryonic charge as a self-interacting fluid. The dynamics reduces to Coleman's false vacuum problem for a scalar field that is a fractional power of that density. The main result is that such a Skyrme-type model is the first one to reproduce, with good accuracy, the experimental values of radii and binding energies for a very wide range of the mass number. The robust and simple properties of the model lead to many possible generalizations with implications not only in nuclear physics but also in other areas of Physics.

¹laf@ifsc.usp.br

²livramento@theor.jinr.ru

1 Introduction

QCD is a quite successful non-abelian gauge theory for the strong interactions of quarks and gluons. It presents asymptotic freedom and it is in very good agreement with experiment at high energies. However, the dynamics of QCD at hadronic scales presents enormous challenges due to its large coupling, and the developments of non-perturbative methods are still well below the needs for an understanding of QCD low energy physics. In order to deal with the massive amount of experimental data, physicists have used all the resources available to construct models for the strong-coupled dynamics among baryons, not necessarily derived from QCD. Nowadays, the state of the art includes, besides lattice gauge theory, *ab initio* models like the no core shell model [1], truncations of it [2], high-low momentum decoupling models [3], as well as low energy effective theories like the inspiring *chiral perturbation theory* put forward by S. Weinberg [4–6]. On the other hand, some important studies on non-abelian gauge theories have shed light on particular sectors of strong-coupled QCD. It has been shown that in the large N -limit, QCD may be equivalent to a theory of mesons, and baryons could be identified with the Skyrmions [7–10].

That observation boosted the interest in an old idea of T. Skyrme, where baryons and nuclei can be interpreted as topological solitons of the so-called Skyrme model [11, 12]. Skyrmion solutions with various baryonic topological charges have been constructed using powerful numerical techniques [13–15]. However, the binding energies obtained are too high when compared with experiment, and that is perhaps linked with the fact that the original Skyrme model does not admit a self-dual sector [16, 17]. Modifications of the Skyrme model leading to self-dual sectors have made some improvement on the problem of the binding energies.

One such attempt reduces self-dual Yang-Mills in four dimensions to a Skyrme model coupled to an infinite tower of vector mesons, with some success for the spectrum of light nuclei [18–20]. Another attempt deals with modifications of the so-called BPS Skyrme model [21, 22] that has obtained reasonable values of binding energies for very heavy nuclei and on some aspects of neutron stars [23, 24]. The Skyrme model has been applied to other aspects of nuclear matter [25, 26], and recently, interesting results were obtained on the spectra of light nuclei [27–30] and on the spin-orbit interaction [31].

In this paper we report results for the values of radii and binding energies for Skyrmions with topological charges varying from 1 to 240, obtained in a modification of the self-dual Skyrme model proposed in [32]. They are in quite good agreement with the experimental values of root-mean-square (rms) charge radii [33] and binding energies per nucleon [34], in a list of $N_c = 265$ nuclei, containing all the stable nuclei up to ^{208}Pb , and above that with those of nuclei up to ^{240}Pu with a half-life greater than 10^3 years, according to [35]. It is the first Skyrme-type model to reproduce those experimental results with a good accuracy and for such a wide range of mass number.

The model that we present is made of two parts. The first one is the self-dual Skyrme model proposed in [32] and further explored in [36], and it consists of a modification of the original Skyrme model [11, 12] where the group indices in the action are contracted, not with the Killing form of $SU(2)$, but with a symmetric matrix h of scalar fields in the quadratic term of the action, and its inverse in the quartic term. It presents an exact self-dual sector

and it is conformally invariant in three space dimensions. The second part is a theory of a self-interacting fluid where the role of the order parameter, denoted ψ , is played by a fractional power of the density of the baryonic (topological) charge. The two parts are coupled through the chiral $SU(2)$ Skyrme fields as the fluid theory does not involve the scalar fields in the matrix h . An interesting aspect of the model is that the h -fields adjust themselves to solve the self-duality equations of the first part of the model, and consequently the $SU(2)$ Skyrme fields are not constrained by the equations of motion coming from that first part. The dynamics of the $SU(2)$ Skyrme fields are determined solely by the equations of the fluid theory.

As a consequence of such interesting coupling, the contribution to the energy of the first part is proportional to the topological charge, as it satisfies the self-duality equations. As such topological charge is the baryonic charge, and so equal to the number of nucleons, it turns out that the energy of the first part gives the masses of the uncoupled nucleons. The contribution to the energy of the self-interacting fluid is responsible for the binding energy of the nucleons inside the nuclei. The two contributions have different energy scales. Such a two scale regime is a desired feature, since it is expected from QCD that nucleons are bound states of quarks and gluons and nuclei are bound states of nucleons, and they involve different energy scales.

The fluid theory have kinetic and potential terms for the order parameter ψ . Since the density of the topological charge involve first derivatives of the $SU(2)$ Skyrme fields, the action of the fluid theory contains second derivatives of those fields. However, due to the topological character of the order parameter ψ , the Euler-Lagrange equations for the $SU(2)$ Skyrme fields, associated to the fluid theory, lead to a second order partial differential equation for ψ . The effect of the third derivative is to introduce an integration constant on those equations, which plays a crucial role in the properties of the model. All the physical properties of the model depend upon such a constant. In particular, the topological charge turns out to be a monotonically decreasing function of it. Such an integration constant plays a role similar to the running coupling constants in the renormalization group. Indeed, we have to choose its value for a reference nucleus in order to fix the value of the physical quantities (mass, baryonic charge, radius, etc) for all other nuclei.

Another interesting feature of the model is that the dynamics of the self-interacting fluid theory reduces to the false vacuum problem of S. Coleman [37, 38]. It follows that the solution for the order parameter ψ that presents the lowest energy, for a given value of the baryonic charge, is the Coleman's bounce solution and so it is spherically symmetric and decays monotonically (exponentially) to zero at large distances. In addition, as the integration constant decreases, and so the baryonic charge increases, the Coleman's false vacuum tend to become degenerate with the true vacuum. A consequence of that is that the order parameter ψ remains practically constant for a large region around the origin, before decaying exponentially to zero at larger distances. Therefore, the heavier the nucleus is, the smaller the value of the corresponding integration constant is, and so the closer it is to that regime. Consequently, such a behavior, together with the spherical symmetry of the solutions, leads in quite natural and robust way to the proportionality between the root mean square (RMS) radius of the nucleus and its baryonic charge risen to the power one third.

The properties of the Coleman’s false vacuum problem also lead to a robust behaviour of the binding energy. We are able to show, for a quite large part of the parameter space of the model, that the binding energy per nucleon, provided by Coleman’s bounce solutions, grows with the baryonic charge and saturates for large values of it. However, the energy functional of the second part of our model possess a topological term which does not affect the equations of motion of the fluid theory. That term can be chosen to be proportional to the square of the baryonic charge and so, for the type of nuclei we consider, it resembles the Coulomb interaction energy among the protons. Therefore, such a topological term will make the binding energy to decrease for large values of the baryonic charge. Consequently, our model reproduces the bulk behaviour of the binding energy per nucleon of a large class of nuclei, for a large portion of parameter space. Those parameters have to be fixed just to fit the scales of the problem, leading to a very good agreement with the experimental data, with errors smaller than 1% for baryonic charges running from 20 to 240, and with even smaller errors for baryonic charges above 60. The error grows a bit for nuclei with baryonic charges between 10 and 20, but not higher than 5%. Only for very light nuclei, with baryonic charges below 10, the error grows to a two digit percentage.

The model describes heavier nuclei better than light ones because of the spherical symmetry of the solutions, imposed by Coleman’s false vacuum problem. In order to improve the description of light nuclei we have perhaps to add kinetic and potentials terms for the scalar fields associated to the symmetric matrix h , in order to break the self-duality. Such a breaking has to be small as the deviations we have from the experimental data are already small. So, such a breaking of self-duality can perhaps be analysed through a perturbative expansion on the couplings constants of such new terms involving the h -fields. In addition, we expect that the breaking of the self-duality will bring the properties of the first part of the model closer to those of the original Skyrme model. Therefore, many results already known for the Skyrme model can perhaps be analysed in the context of the present model.

The paper is organised as follows. In section 2 we introduce our model, made of the self-dual Skyrme model, introduced in [32, 36], coupled to a self-interacting fluid with an order parameter which is a fractional power of the density of baryonic charge. In section 3 we show that the dynamics of the fluid theory reduces to the Coleman’s false vacuum problem [37, 38] and discuss its consequences. The analysis of the bulk properties of the binding energy per nucleon is made in section 4. The choice of an admissible potential, in the sense of [37, 38], is made in section 5, and it is shown that the model presents a robust behaviour that agrees with the bulk properties of nuclei. The analysis of the numerical and experimental data is made in section 6, and our conclusions are presented in section 7. In the Appendix A we describe our numerical methods, and in the Appendix B we provide a long table with the detailed numerical and experimental data used in the analysis of section 6.

2 The model

The first part of our model consists of a modified Skyrme model [32, 36] containing, besides the usual chiral fields $U \in SU(2)$, six scalar fields assembled in a 3×3 , symmetric and

invertible matrix h_{ab} , with all its eigenvalues being positive, and defined by the static energy

$$E_1 = \int d^3x \left[\frac{m_0^2}{2} h_{ab} R_i^a R_i^b + \frac{1}{4e_0^2} h_{ab}^{-1} H_{ij}^a H_{ij}^b \right] \quad (2.1)$$

where m_0 and e_0 are coupling constant with dimension of $[m_0] = \sqrt{[\text{energy}]/[\text{length}]}$ and $[e_0] = 1/\sqrt{[\text{energy}][\text{length}]}$. In addition,

$$R_\mu^a = i \widehat{\text{Tr}} (\partial_\mu U U^\dagger T_a); \quad H_{\mu\nu}^a = \varepsilon_{abc} R_\mu^b R_\nu^c \quad (2.2)$$

with T_a , $a = 1, 2, 3$, being the basis of the $SU(2)$ Lie algebra satisfying $[T_a, T_b] = i \varepsilon_{abc} T_c$, and $\widehat{\text{Tr}}(T_a T_b) = \delta_{ab}$, is a normalised trace. In a given representation of $SU(2)$ we have that $\text{Tr}(T_a T_b) = k \delta_{ab}$, with k being proportional to the Dynkin index of that representation. We define $\widehat{\text{Tr}} \equiv \frac{1}{k} \text{Tr}$. Following the ideas of [39], the introduction of h_{ab} makes possible the existence of a self-dual sector [40, 41]. The self-duality equations are given by

$$\lambda h_{ab} R_i^b = \frac{1}{2} \varepsilon_{ijk} H_{jk}^a \quad \text{with} \quad \lambda = \pm m_0 e_0 \quad (2.3)$$

The sign of λ characterises the self-dual and anti-self-dual sectors of (2.1), and the solutions on those sectors saturate a bound on the energy, such that

$$E_1 = 48 \pi^2 \frac{m_0}{e_0} |Q| \quad (2.4)$$

where Q is the topological charge of the Skyrme model, i.e.

$$Q = \frac{i}{48 \pi^2} \int d^3x \varepsilon_{ijk} \widehat{\text{Tr}}(R_i R_j R_k) \quad (2.5)$$

with $R_i = R_i^a T_a$. It follows from self-duality that

$$\text{sign}(\lambda Q) = -1 \quad (2.6)$$

The introduction of h_{ab} also renders the theory (2.1) conformally invariant in the three dimensional space [32, 36].

The results of [36] relevant for the construction of the model proposed in this paper are: *i*) the first order self-duality equations (2.3) imply the nine static second order Euler-Lagrange equations associated to fields U and h_{ab} , *ii*) the static Euler-Lagrange equations associated to the fields h_{ab} are equivalent to the self-duality equations, *iii*) given a configuration for the U -fields one can solve the self-duality equations by taking h_{ab} to be

$$h = \frac{\sqrt{\det \tau}}{m_0 e_0} \tau^{-1}; \quad \tau_{ab} = R_i^a R_i^b \quad (2.7)$$

So, the fields h_{ab} are spectators in the sense that they adjust themselves to solve the self-duality equations for any configuration of the U -fields. Note that the matrix τ is similar to the Skyrme model strain tensor [15]. For U -field configurations where τ is singular the

matrix h_{ab} still solves the self-duality equation but it is not completely determined by U , and have some arbitrary components [36].

Therefore, if one modifies the theory (2.1) by adding a static energy E_2 that depends only on the U -fields, the Euler-Lagrange equations associated to the h -fields will not change and so the self-duality equations will continue to be valid, and consequently the matrix h will be determined from the U -fields. In addition, the part of the Euler-Lagrange equations associated to the U -fields coming from E_1 will be automatically satisfied, since the self-duality equations still hold true. So, the configurations of the U -fields will only be subjected to the E_2 -part of their Euler-Lagrange equations. Consequently, the addition of such U -dependent E_2 , may break the conformal symmetry of the theory (2.1), but will keep its self-dual sectors intact. So, using (2.4), the static energy of our model is given by

$$E = 48 \pi^2 \frac{m_0}{e_0} |Q| + E_2 \quad (2.8)$$

and we shall take E_2 to be a fluid theory for a quantity ψ which is proportional to a fractional power of the density of the topological charge, i.e.

$$\psi^s \equiv -\frac{i}{12\lambda^3} \varepsilon_{ijk} \widehat{\text{Tr}}(R_i R_j R_k) \quad (2.9)$$

with s being a real positive parameter. The introduction of λ in (2.9) makes ψ to be dimensionless and positive. The self-duality equation implies that $\det h = 4\psi^s$ [36], and so the positivity of ψ follows from the fact that the eigenvalues of h are positive in order for E_1 to be positive. We take E_2 to be

$$E_2 = \int d^3x \left[\frac{\mu_0^2}{2} (\partial_i \psi)^2 + V(\psi) + G(U) \psi^s \right] \quad (2.10)$$

where μ_0 is a coupling constant with dimension of mass, and $G(U)$ is a functional of the U -fields but not of their derivatives, which we shall take to be positive. Note that the G -term in (2.10) is topological in the sense that it is invariant under any smooth variation of the U -fields. It differs from the Skyrme topological charge Q since G works like a deformation of the target space and may break the $SU(2)_L \otimes SU(2)_R$ symmetry of (2.1). Since ψ depends upon the first derivatives of the U -fields, it follows that E_2 presents second derivatives of those fields. However, the Euler-Lagrange equations for the U -fields take a simple form in terms of ψ . In order to see that, it is easier to use Darboux-like coordinates on $SU(2)$ given by

$$U = \begin{pmatrix} \sqrt{1-F} e^{i\theta_2} & i\sqrt{F} e^{i\theta_1} \\ i\sqrt{F} e^{-i\theta_1} & \sqrt{1-F} e^{-i\theta_2} \end{pmatrix}; \quad 0 \leq F \leq 1; \quad 0 \leq \theta_1, \theta_2 \leq 2\pi \quad (2.11)$$

and (2.9) becomes

$$\psi^s = \frac{1}{\lambda^3} \varepsilon_{ijk} \partial_i F \partial_j \theta_1 \partial_k \theta_2 \quad (2.12)$$

Then the Euler-Lagrange equations following from (2.10), associated to the fields F , θ_1 and θ_2 are, respectively,

$$\varepsilon_{ijk} \partial_j \theta_1 \partial_k \theta_2 \partial_i \left[\psi^{1-s} \left(-\mu_0^2 \partial_l^2 \psi + \frac{\delta V}{\delta \psi} \right) \right] = 0$$

$$\begin{aligned}\varepsilon_{ijk} \partial_i F \partial_k \theta_2 \partial_j \left[\psi^{1-s} \left(-\mu_0^2 \partial_l^2 \psi + \frac{\delta V}{\delta \psi} \right) \right] &= 0 \\ \varepsilon_{ijk} \partial_i F \partial_j \theta_1 \partial_k \left[\psi^{1-s} \left(-\mu_0^2 \partial_l^2 \psi + \frac{\delta V}{\delta \psi} \right) \right] &= 0\end{aligned}\tag{2.13}$$

Therefore, it turns out that the three Euler-Lagrange associated to the U -fields are equivalent to

$$\mu_0^2 \partial^2 \psi - \frac{\delta V_{\text{eff.}}}{\delta \psi} = 0; \quad V_{\text{eff.}} \equiv V - c \psi^s \tag{2.14}$$

where c is an arbitrary integration constant. Clearly, if we take ψ as the fundamental degree of freedom, instead of the U -fields, (2.14) is the Euler-Lagrange equation following from the functional

$$E_{\text{eff.}} = \int d^3x \left[\frac{\mu_0^2}{2} (\partial_i \psi)^2 + V(\psi) - c \psi^s \right] \tag{2.15}$$

The equation (2.14) is the only one we have to solve to construct the Skyrmions, and for each choice of c there will be at least one solution. The subtlety however is that the acceptable solutions are those such that the Skyrme topological charge

$$Q = -\frac{\lambda^3}{4\pi^2} \int d^3x \psi^s \tag{2.16}$$

is an integer, otherwise we will not be able to integrate (2.9) to obtain the solution for the U -fields with the appropriate boundary conditions. The parameter c therefore plays the role of a running coupling constant, and we will have to choose which value of it corresponds to a chosen value of the topological charge. Once that choice is made the allowed values of c will fall into a discrete sequence of real numbers.

Note that from (2.6) it follows that

$$|Q| = \frac{|\lambda|^3}{4\pi^2} \int d^3x \psi^s \tag{2.17}$$

3 The false vacuum

Obviously, the density of baryonic charge must go to zero at infinity, and so we need $\psi \rightarrow 0$ as $r \rightarrow \infty$. Therefore, $\psi = 0$ must be an extrema of $V_{\text{eff.}}$. In addition, in order to have $E_{\text{eff.}}$ finite we need $V_{\text{eff.}}$ to vanish at $\psi = 0$. So we need

$$\psi|_{r \rightarrow \infty} = 0; \quad V_{\text{eff.}}|_{\psi=0} = 0; \quad \frac{\delta V_{\text{eff.}}}{\delta \psi}|_{\psi=0} = 0 \tag{3.1}$$

A quite robust property of nuclei is that the nuclear matter density ρ falls exponentially at large distances as $\rho(r) \sim \rho_0 e^{-r/a}$, with a being roughly independent of the mass number and given approximately by $a = 0.524$ Fermi. Our model does have the property that all

solutions, with any value of the baryonic charge, fall off exponentially at the same rate. From (2.9) we must identify ρ with ψ^s . Therefore, expanding (2.14) around $\psi = 0$, one observes that ψ behaves as

$$\psi \sim \frac{e^{-r/(sa)}}{r}; \quad \text{for } r \rightarrow \infty \quad (3.2)$$

if we assume that

$$\frac{\delta^2 V_{\text{eff.}}}{\delta \psi^2} \big|_{\psi=0} = \left(\frac{\mu_0}{s a} \right)^2 \quad (3.3)$$

So, $\psi = 0$ must be a local minimum of $V_{\text{eff.}}$.

The solutions of (2.14) must be stable under Derrick's argument [38, 42]. Indeed, writing (2.15) as

$$E_{\text{eff.}} = T + U_{\text{eff.}}; \quad T = \frac{\mu_0^2}{2} \int d^3x (\partial_i \psi)^2; \quad U_{\text{eff.}} = \int d^3x V_{\text{eff.}} \quad (3.4)$$

and defining the scale transformation $\psi_\alpha(x) = \psi(x/\alpha)$, we have that $T \rightarrow \alpha T$ and $U_{\text{eff.}} \rightarrow \alpha^3 U_{\text{eff.}}$. Any solution of (2.14) makes $E_{\text{eff.}}$ stationary, and so $E_{\text{eff.}}$ should be stationary under scale transformation when (2.14) is imposed. Therefore, we must have

$$T + 3 U_{\text{eff.}} = 0; \quad \text{and so} \quad E_{\text{eff.}} = \frac{2}{3} T \quad (3.5)$$

Thus, $E_{\text{eff.}}$ is positive and $U_{\text{eff.}}$ is negative when evaluated on solutions of (2.14). That means $V_{\text{eff.}}$ must be negative for some region of values of ψ . We are then led to S. Coleman's false vacuum problem [37, 38]. The main result of [38] is that, for what it defines as an admissible effective potential $V_{\text{eff.}}$, the equation (2.14) possesses at least one monotone spherically symmetric solution ψ_c vanishing at infinity, other than the trivial solution $\psi = 0$. In addition, this solution has an effective energy $E_{\text{eff.}}(\psi_c)$ that is less than or equal to that of any other solution vanishing at infinity. Any other solution vanishing at infinity which is not both spherically symmetric and monotone has an effective energy that is strictly greater than $E_{\text{eff.}}(\psi_c)$.

Note that E_2 and $E_{\text{eff.}}$ differ by the topological term $\int d^3x (G + c) \psi^s$, which is constant within a given homotopy class. Therefore, the minima of E_2 for a given value of the Skyrme topological charge Q correspond to the minima of $E_{\text{eff.}}$ for that same value of Q . Consequently, the minima of E_2 are monotone and spherically symmetric too. Due to such spherical symmetry we shall use an holomorphic ansatz for the U -fields in terms of a radial profile function $f(r)$, and a complex scalar field u depending upon the angles, i.e.

$$U = W^\dagger e^{i f T_3} W, \quad \text{with} \quad W = \frac{1}{\sqrt{1 + |u|^2}} \begin{pmatrix} 1 & i u \\ i \bar{u} & 1 \end{pmatrix} \quad (3.6)$$

For such a type of configuration, the self-duality equations are satisfied by an h -matrix of the form $h = d(V) h_D d^T(V)$, where $d(V)$ is the adjoint (triplet) representation of the group element $V = W^\dagger e^{i f T_3/2}$, with

$$h_D = (f'(r)/\lambda) \text{diag.} \left[1, 1, \frac{4 \sin^2(f/2)}{r^2 f'^2} \right] \quad (3.7)$$

and where we have chosen $u = (x_2 + i x_1) / (r - x_3)$ (see [36]). In order for the baryonic charge Q to be positive (see (2.6)) we shall choose the self-dual sector where $\lambda = -m_0 e_0 < 0$, and so f is a monotonically decreasing function of r . From (2.9), or equivalently $\det h = 4 \psi^s$, we get that

$$\psi^s = -(m_0 e_0)^{-3} \frac{1}{2 r^2} \frac{d}{d r} [f - \sin f] \quad (3.8)$$

which leads, for the boundary conditions $f(0) = 2\pi |Q|$ and $f(\infty) = 0$, to a positive Skyrme topological charge. Note that this does not imply that we are considering the Skyrme product ansatz, since $f_{|Q|} \neq |Q| f_1$, and so $U_{|Q|} \neq U_1^{|Q|}$. Note that negative topological charges can be obtained by choosing the other self-dual sector where $\lambda > 0$ and f is a monotonically increasing function of r . In both cases ψ and the eigenvalues of h are positive. So far, the results do not depend upon the detailed form of the effective potential, as long as it is admissible in the sense of [38].

Coleman's false vacuum argument has established that, for each sector of topological charge Q , the minimum of the energy E_2 , given in (2.10), has to be spherically symmetric and monotone. Therefore, (2.14) reduces to an ordinary differential equation for a radial function $\psi(r)$, i.e.

$$\mu_0^2 \left[\frac{d^2 \psi}{dr^2} + \frac{2}{r} \frac{d\psi}{dr} \right] - \frac{\delta V_{\text{eff.}}}{\delta \psi} = 0 \quad (3.9)$$

and $V_{\text{eff.}}$ has to be negative for some interval of values of ψ . Since we want E_2 to be positive, we shall take V to be positive. Therefore, the integration constant c has to be positive. In order to comply with (3.1) and (3.3) we shall take

$$V_{\text{eff.}} = \beta_2^2 \psi^2 - c \psi^s + \tilde{V}; \quad 2 < s < 6 \quad (3.10)$$

and

$$\tilde{V} \geq 0; \quad \tilde{V}|_{\psi=0} = 0; \quad \frac{\delta \tilde{V}}{\delta \psi}|_{\psi=0} = 0; \quad \frac{\delta^2 \tilde{V}}{\delta^2 \psi}|_{\psi=0} = 0 \quad (3.11)$$

For sufficiently large c the effective potential $V_{\text{eff.}}$ will certainly be negative in some region of ψ , and so $V_{\text{eff.}}$ will be admissible in the sense of [38]. However, there is a non-negative critical value $c_{\text{crit.}}$ such that for $c < c_{\text{crit.}}$ the effective potential will be positive everywhere and Coleman's false vacuum solution ceases to exist.

Note that Coleman's false vacuum solution can exist even for the cases where $c \psi^s > \tilde{V}$, for $\psi \rightarrow \infty$, and so $V_{\text{eff.}}$ is unbounded from below. In such cases we have $c_{\text{crit.}} = 0$, and for the solutions corresponding to c approaching such $c_{\text{crit.}}$, the value of ψ , at $r = 0$, diverges. We shall not consider such situation as we do not want divergent values of the baryonic charge density. Consequently, we shall consider the cases where $c \psi^s < \tilde{V}$, for $\psi \rightarrow \infty$, and so $V_{\text{eff.}}$ is bounded from below. Therefore, $V_{\text{eff.}}$ has a true global vacuum $\psi_{\text{vac.}}$, such that

$$\frac{\delta V_{\text{eff.}}}{\delta \psi}|_{\psi_{\text{vac.}}} = 0; \quad V_{\text{eff.}}(\psi_{\text{vac.}}) < 0 \quad (3.12)$$

As c decreases such a vacuum becomes shallow and at a critical value $c_{\text{crit.}} > 0$, it becomes degenerated with the false vacuum $\psi = 0$, i.e. $\psi_{\text{vac.}} \rightarrow \psi_{\text{crit.}}$, such that $V_{\text{eff.}}(\psi_{\text{crit.}}) = 0$. At

this point Coleman's false vacuum solution ceases to exist, and one gets instead a constant solution $\psi = \psi_{\text{crit.}}$, with divergent value of the integrated baryonic charge, i.e. $Q \rightarrow \infty$.

As Coleman points out [37, 38], one can analyse (3.9) as the problem of a mechanical particle with position being given by the coordinate ψ , as a function of the time r , and moving under the influence of the inverted potential $V_{\text{eff.}}^{(-)} \equiv -V_{\text{eff.}}$, and of a viscous force $-\mu_0^2 \frac{2}{r} \frac{d\psi}{dr}$. Multiplying (3.9) by $\frac{d\psi}{dr}$, one gets that

$$\frac{d\mathcal{E}_{\text{particle}}}{dr} = -\mu_0^2 \frac{2}{r} \left(\frac{d\psi}{dr} \right)^2 \quad (3.13)$$

with

$$\mathcal{E}_{\text{particle}} = \frac{\mu_0^2}{2} \left(\frac{d\psi}{dr} \right)^2 + V_{\text{eff.}}^{(-)} \quad (3.14)$$

By expanding (3.9) around $r = 0$ one concludes that $\frac{d\psi}{dr} \big|_{r=0} = 0$. From (3.13) one observes that as the particle moves from $r = 0$, the energy $\mathcal{E}_{\text{particle}}$ only decreases. Therefore, we have to release the particle at $r = 0$, from a position ψ_0 , such that $\mathcal{E}_{\text{particle}}(0) = V_{\text{eff.}}^{(-)}(\psi_0) > 0$, and so with ψ_0 inside the interval where $V_{\text{eff.}}$ is negative. The Coleman's false vacuum solution will end, as $r \rightarrow \infty$, at $\psi = 0$, with zero velocity $\frac{d\psi}{dr}$, and so with zero energy $\mathcal{E}_{\text{particle}}$. So, we have that

$$\mathcal{E}_{\text{particle}}(0) = V_{\text{eff.}}^{(-)}(\psi_0) = \mu_0^2 \int_0^\infty dr \frac{2}{r} \left(\frac{d\psi}{dr} \right)^2 \quad (3.15)$$

Note that as c approaches $c_{\text{crit.}}$, from above, one has that $\psi_0 \rightarrow \psi_{\text{crit.}}$, and so $V_{\text{eff.}}^{(-)}(\psi_0) \rightarrow 0$. As the integrand on the l.h.s of (3.15) is positive, one observes that it will have to go to zero everywhere as $c \rightarrow c_{\text{crit.}}$, from above. But Coleman's false vacuum solutions eventually decay, at large distances, to the false vacuum $\psi = 0$, within a length scale a , which is independent of c , as given in (3.2). Since $\frac{d\psi}{dr}$ is non-vanishing in that region, one observes that as $c \rightarrow c_{\text{crit.}}$, that decay will happen for larger and larger values of r , in order for the factor $\frac{2}{r}$, in the integrand on the l.h.s of (3.15), to suppress the derivative of ψ . Therefore, the solutions, for c close to $c_{\text{crit.}}$, develop a plateau from $r = 0$ to $r = R(c)$, where ψ is practically constant, and they decay to the false vacuum for $r > R(c)$. Note however that $R(c)$ grows as c decreases towards $c_{\text{crit.}}$. In addition, the value of ψ on the plateau approaches $\psi_{\text{crit.}}$ as $c \rightarrow c_{\text{crit.}}$.

From (2.16) we have that

$$Q \sim \int d^3x \psi^s \sim \psi_0^s \int_0^{R(c)} dr r^2 \sim \frac{1}{3} R(c)^3 \psi_0^s \quad (3.16)$$

One then observes that the baryonic charge Q grows as c decreases towards $c_{\text{crit.}}$. In addition, the root mean square (RMS) radius of the solution becomes

$$\sqrt{\langle r \rangle} = \sqrt{\frac{\int d^3x r^2 \psi^s}{\int d^3x \psi^s}} \sim \sqrt{\frac{3}{5}} R(c); \quad \rightarrow \quad \sqrt{\langle r \rangle} \sim Q^{1/3} \quad (3.17)$$

Consequently, the solutions for c close to $c_{\text{crit.}}$ tend to satisfy a linear relation between the RMS radius and $Q^{1/3}$, which is the power law one observes experimentally for nuclei above some baryonic charge (mass number).

One observes that the false vacuum solution presents some robust properties, which are quite independent of the value of the parameters of the model. First, the baryonic charge decreases with the increase of the integration constant c . Second, the relation between RMS radius and baryonic charge obeys the relation $\sqrt{\langle r \rangle} \sim Q^{1/3}$. Those two properties are valid as c approaches $c_{\text{crit.}}$. However, as we will see below, the range of c where such properties are valid is large enough to accommodate most of the nuclei. The discrepancies are relevant for baryonic charge below 12.

4 The binding energy per nucleon

Another important property of our model is that the binding energy per nucleon presents a very robust dependency upon the baryonic charge, for a quite large portion of the parameter space. As we have argued at the end of section 3, the baryonic charge Q is a monotonic decreasing function of the integration constant c , at least for a region where c approaches the critical value $c_{\text{crit.}}$ where the Coleman's false vacuum solution ceases to exist. Assuming that dependency of Q upon c , and for some suitable region of the parameters in $G(U)$ (see (2.10)), we show that the binding energy per nucleon increases with Q , for small values of Q , up to a maximum, and then decreases with Q , for large values of the baryonic charge.

As we have seen, Derrick's scaling argument leads to the relation (3.5) between the kinetic energy T and the effective potential energy $U_{\text{eff.}}$. Combining (3.5) with the relation between V and $V_{\text{eff.}}$, given in (2.14), we replace the integral of V in E_2 , given in (2.10), by $\int d^3x V = \int d^3x (V_{\text{eff.}} + c \psi^s) = -\frac{T}{3} + c \int d^3x \psi^s$, and so

$$E_2 = \frac{2}{3} T + \frac{4\pi^2}{|\lambda|^3} c |Q| + Q_G \quad (4.1)$$

where we have used (2.17) and have denoted

$$Q_G = \int d^3x G(U) \psi^s \quad (4.2)$$

For a given potential V , the solutions of (2.14) are functions of the integration constant c . Therefore, differentiating E_2 , given in (2.10), w.r.t. c and integrating by parts we get

$$\frac{dE_2}{dc} = \int d^3x \left[\mu_0^2 \partial_i \left(\partial_i \psi \frac{d\psi}{dc} \right) - \mu_0^2 \partial^2 \psi \frac{d\psi}{dc} + \frac{\delta V}{\delta \psi} \frac{d\psi}{dc} \right] + \frac{dQ_G}{dc} \quad (4.3)$$

Since $\psi \rightarrow 0$, and $\partial_i \psi \rightarrow 0$ as $r \rightarrow \infty$, in order for the density of baryonic charge to vanish at infinity, we get that the first term on the r.h.s. of (4.3) vanishes. Using, on the second term of (4.3), the equation (2.14), and also (2.17), we get that

$$\frac{dE_2}{dc} = \frac{4\pi^2}{|\lambda|^3} c \frac{d|Q|}{dc} + \frac{dQ_G}{dc} \quad (4.4)$$

The binding energy per nucleon is

$$E_B = \frac{|Q| E(Q=1) - E(|Q|)}{|Q|} = \frac{|Q| E_2(Q=1) - E_2(|Q|)}{|Q|} \quad (4.5)$$

with E given in (2.8). Therefore, using (4.1) and (4.4) one gets

$$\frac{dE_B}{dc} = \frac{2}{3} \frac{T}{|Q|^2} \frac{d|Q|}{dc} - \frac{1}{|Q|^2} \left[|Q| \frac{dQ_G}{dc} - Q_G \frac{d|Q|}{dc} \right] \quad (4.6)$$

If the relation between Q and c is invertible, i.e. one is a monotonic function of the other, we can write (4.6) as

$$\frac{dE_B}{d|Q|} = \frac{2}{3} \frac{T}{|Q|^2} - \frac{1}{|Q|^2} \left[|Q| \frac{dQ_G}{d|Q|} - Q_G \right] \quad (4.7)$$

In order for E_2 to be positive we shall take the potential V to be non-negative. However, the Derrick's scaling argument implies (3.5), and so $U_{\text{eff.}}$ has to be negative, as T is always positive, and so $V_{\text{eff.}}$ has to be negative in some region of the ψ -axis. The only way to achieve that is to have the integration constant c to be positive, as ψ is positive. From (3.5) we have that

$$\frac{T}{3} = \frac{4\pi^2}{|\lambda|^3} c |Q| - \int d^3x V > 0 \quad \rightarrow \quad \frac{4\pi^2}{|\lambda|^3} c |Q| > \int d^3x V \quad (4.8)$$

Therefore

$$T = \frac{12\pi^2}{|\lambda|^3} c |Q| \Omega \quad \text{with} \quad \Omega = 1 - \frac{|\lambda|^3}{4\pi^2} \frac{1}{c |Q|} \int d^3x V < 1 \quad (4.9)$$

We then conclude that

$$0 < \frac{T}{|Q|^2} < \frac{12\pi^2}{|\lambda|^3} \frac{c}{|Q|} \quad (4.10)$$

The type of nuclei we shall consider are such that the number of protons and neutrons do not differ drastically, and so, the charges of such nuclei are approximately proportional to $|Q|$. Therefore, we shall choose the functional $G(U)$ such that Q_G is positive and proportional to $|Q|^2$, i.e. $Q_G = \chi |Q|^2$ ($\chi > 0$), and so Q_G approximates the Coulomb interaction energy for the nuclei. Then, (4.7) becomes

$$\frac{dE_B}{d|Q|} = \frac{2}{3} \frac{T}{|Q|^2} - \chi \quad (4.11)$$

In order to obtain (4.7) we have assumed that c is a monotonic function of $|Q|$. If we go further and assume that c is a monotonically decreasing function of $|Q|$, we can get, from (4.10) and (4.11), the bulk of the form of the binding energy per nucleon as a function of $|Q|$. Indeed, with an appropriate value for χ , we get that for sufficiently small values of $|Q|$ we have that $\frac{2}{3} \frac{T}{|Q|^2} > \chi$, and so E_B grows with the increase of $|Q|$, and for sufficiently large values of $|Q|$, we get that $\frac{2}{3} \frac{T}{|Q|^2} < \chi$, and so E_B decreases with the increase of $|Q|$. However, with such analysis we can not rule out local minima and maxima of E_B .

We have shown, at the end of section 3, that the baryonic charge Q is a monotonic decreasing function of the integration constant c , at least for a region where c approaches the critical value $c_{\text{crit.}}$. As we will see below, that region can be large enough to accommodate all nuclei. Therefore the dynamics of our model leads in a quite robust way for a binding energy per nucleon that reproduces the bulk of the features of the experimental data. The choice of the parameters of V and $G(U)$ can be used to match the scales and so to fine tune that experimental data, as we now explain.

5 Choice of the potential

We shall consider the following potential, admissible in the sense of [37, 38],

$$V_{\text{eff.}} = \beta_2^2 \psi^2 - c \psi^s + \beta_\kappa^2 \psi^\kappa; \quad 6 > s > 2; \quad \kappa > s \quad (5.1)$$

with the ratio μ_0/β_2 determined from (3.3), as

$$\frac{\mu_0}{\beta_2} = \sqrt{2} s a \quad (5.2)$$

In order to better analyze the role of the parameters of the model, let us define the dimensionless quantities

$$\zeta = \frac{\beta_2}{\mu_0} r; \quad \widehat{\psi} = \left(\frac{\beta_\kappa}{\beta_2^2} \right)^{\frac{1}{(\kappa-2)}} \psi; \quad \gamma = \frac{c}{\beta_2^2} \left(\frac{\beta_2^2}{\beta_\kappa^2} \right)^{\frac{s-2}{\kappa-2}} \quad (5.3)$$

According to Coleman's false vacuum argument the solution of (2.14) with smallest energy has to be radial, and so using (5.3), one gets that (2.14) becomes

$$\frac{d^2 \widehat{\psi}}{d\zeta^2} + \frac{2}{\zeta} \frac{d\widehat{\psi}}{d\zeta} - \frac{\delta \widehat{V}_{\text{eff.}}}{\delta \widehat{\psi}} = 0; \quad \widehat{V}_{\text{eff.}} = \widehat{V} - \gamma \widehat{\psi}^s = \widehat{\psi}^2 - \gamma \widehat{\psi}^s + \widehat{\psi}^\kappa \quad (5.4)$$

In addition, the topological charge becomes

$$|Q| = \left(\frac{\mu_0}{\beta_2} \right)^3 \vartheta I(\gamma, s, \kappa) \quad (5.5)$$

with

$$\vartheta = (m_0 e_0)^3 \left(\frac{\beta_2^2}{\beta_\kappa^2} \right)^{\frac{s}{(\kappa-2)}} \quad I = \frac{1}{\pi} \int_0^\infty d\zeta \zeta^2 \widehat{\psi}^s \quad (5.6)$$

Therefore, the density of baryonic charge becomes

$$\rho = \frac{\vartheta}{4\pi^2} \widehat{\psi}^s \quad \text{with} \quad |Q| = \int d^3x \rho \quad (5.7)$$

The root-square-mean radius of the baryonic charge is

$$\sqrt{\langle r^2 \rangle} \equiv \sqrt{\frac{\int d^3x r^2 \psi^s}{\int d^3x \psi^s}} = \frac{\mu_0}{\beta_2} \Lambda(\gamma, s, \kappa) \quad (5.8)$$

with

$$\Lambda \equiv \sqrt{\frac{J(\gamma, s, \kappa)}{I(\gamma, s, \kappa)}}; \quad J = \frac{1}{\pi} \int_0^\infty d\zeta \zeta^4 \widehat{\psi}^s \quad (5.9)$$

We look for solutions of (5.4) satisfying $\widehat{\psi}'(0) = 0$ and $\widehat{\psi}(\infty) = \widehat{\psi}'(\infty) = 0$. For given values of κ and s , we can vary the parameter γ , which has been traded by the arbitrary integration

constant c , and obtain solutions of any baryonic charge. Note that the ratio μ_0/β_2 gives only the scale of the rms radii (5.8) and the shape is given only by $\Lambda(s, \kappa, \gamma)$.

Note that $\widehat{\psi} = 0$ is a local minimum of the effective potential (5.1), i.e. the false vacuum. The global minimum, or the true vacuum, occurs for some positive value of $\widehat{\psi}$. However, as γ decreases there will be a critical value $\gamma_{\text{crit.}}$ such that the true vacuum becomes degenerated with the false vacuum, and Coleman's false vacuum solution ceases to exist, as we discussed in section 3. That happens when

$$V_{\text{eff.}}|_{\gamma_{\text{crit.}}, \widehat{\psi}_{\text{crit.}}} = 0; \quad \frac{\delta V_{\text{eff.}}}{\delta \widehat{\psi}}|_{\gamma_{\text{crit.}}, \widehat{\psi}_{\text{crit.}}} = 0 \quad (5.10)$$

which implies

$$\gamma_{\text{crit.}} = \left(\frac{\kappa - 2}{\kappa - s} \right) \left(\frac{\kappa - s}{s - 2} \right)^{\frac{s-2}{\kappa-2}}; \quad \widehat{\psi}_{\text{crit.}} = \left(\frac{s - 2}{\kappa - s} \right)^{\frac{1}{\kappa-2}} \quad (5.11)$$

5.1 The bulk properties of the model

Given the values of s and κ we can solve the equation (5.4) to find Coleman's false vacuum solution $\widehat{\psi}$, for several values of the re-scaled integration constant γ . Then we can evaluate the quantities I and Λ , given in (5.6) and (5.9) respectively, which are the re-scaled baryonic charge $|Q|$ and root-square-mean radius $\sqrt{\langle r^2 \rangle}$, respectively.

In Figures 1, 2 and 3, we plot $\ln(I)$ against $1/\gamma$, for several values of s and κ . One can clearly observe that the quantity I , and so the baryonic charge $|Q|$, is a monotonically decreasing function of the re-scaled integration constant γ . In addition, the quantity I grows very fast as the integration constant γ decreases to its critical value $\gamma_{\text{crit.}}$, given in (5.11). For very large values of γ , the quantity I becomes very small and insensitive to the value of κ . Indeed, that can be understood from the equation (5.4) for $\widehat{\psi}$. Re-scale $\widehat{\psi}$ as

$$\bar{\psi} = \gamma^{1/(s-2)} \widehat{\psi} \quad (5.12)$$

Then, (5.4) becomes

$$\frac{d^2 \bar{\psi}}{d\zeta^2} + \frac{2}{\zeta} \frac{d\bar{\psi}}{d\zeta} = 2\bar{\psi} - s\bar{\psi}^{s-1} + \frac{\kappa}{\gamma^{(\kappa-2)/(s-2)}} \bar{\psi}^{\kappa-1} \quad (5.13)$$

Since we are assuming $\kappa > s$ (see (5.1)), we observe that in the limit $\gamma \rightarrow \infty$, the term $\bar{\psi}^{\kappa-1}$ decouples from the equation, and the solutions of (5.13) depend upon s only. As we are assuming $s > 2$ (see (5.1)) we get from (5.12) that for $\bar{\psi}$ to be finite one needs $\widehat{\psi} \rightarrow 0$, as $\gamma \rightarrow \infty$. So, indeed $I \rightarrow 0$, as $\gamma \rightarrow \infty$, as we observe from Figures 1, 2 and 3.

The root-square-mean radius of the baryonic charge, given in (5.8), becomes

$$\sqrt{\langle r^2 \rangle}|_{\gamma \rightarrow \infty} = \sqrt{\frac{\int d^3x r^2 \psi^s}{\int d^3x \psi^s}}|_{\gamma \rightarrow \infty} = \frac{\mu_0}{\beta_2} \bar{\Lambda}(s) \equiv r_{\text{min.}}(s) \quad (5.14)$$

with

$$\bar{\Lambda} \equiv \sqrt{\frac{\bar{J}(s)}{\bar{I}(s)}}; \quad \bar{I}(s) = \frac{1}{\pi} \int_0^\infty d\zeta \zeta^2 \bar{\psi}^s; \quad \bar{J}(s) = \frac{1}{\pi} \int_0^\infty d\zeta \zeta^4 \bar{\psi}^s; \quad \gamma \rightarrow \infty \quad (5.15)$$

Note that using the relations (5.5), (5.8) and (5.14) we can express the rms radius as

$$\sqrt{\langle r^2 \rangle} = r_{\min.}(s) + \vartheta^{-1/3} \Omega(\gamma, s, \kappa) |Q|^{1/3} \quad (5.16)$$

with

$$\Omega(\gamma, s, \kappa) \equiv \sqrt{\frac{J(\gamma, s, \kappa)}{I^{5/3}(\gamma, s, \kappa)}} - \frac{\bar{\Lambda}(s)}{I^{1/3}(\gamma, s, \kappa)} \quad (5.17)$$

Note that

$$\Omega(\gamma, s, \kappa) \rightarrow 0; \quad \text{as} \quad \gamma \rightarrow \infty \quad (5.18)$$

For $\gamma = \gamma_{\text{crit.}}$ we get that $\hat{\psi}$ becomes constant and equal to $\hat{\psi}_{\text{crit.}}$ given by (5.11). Therefore,

$$J \rightarrow \frac{\hat{\psi}_{\text{crit.}}^s}{\pi} \int_0^R d\zeta \zeta^4; \quad I \rightarrow \frac{\hat{\psi}_{\text{crit.}}^s}{\pi} \int_0^R d\zeta \zeta^2; \quad \text{for} \quad R \rightarrow \infty \quad (5.19)$$

and so

$$\Omega(\gamma_{\text{crit.}}, s, \kappa) = \sqrt{\frac{3^{5/3}}{5}} \pi^{1/3} \left(\frac{\kappa - s}{s - 2} \right)^{\frac{s}{3(\kappa - 2)}} \quad (5.20)$$

Note that such results are valid for any choice of the coupling constants, and so the fact that the baryonic charge $|Q|$ is a monotonically decreasing function of γ , is a quite robust property of our model. Such property was the basic assumption we have made in section 4 to show that the binding energy per nucleon has the desired dependency upon the baryonic charge. The choice of the values of the coupling constants will be necessary solely to fix the scales, and not the bulk behavior of the binding energy per nucleon.

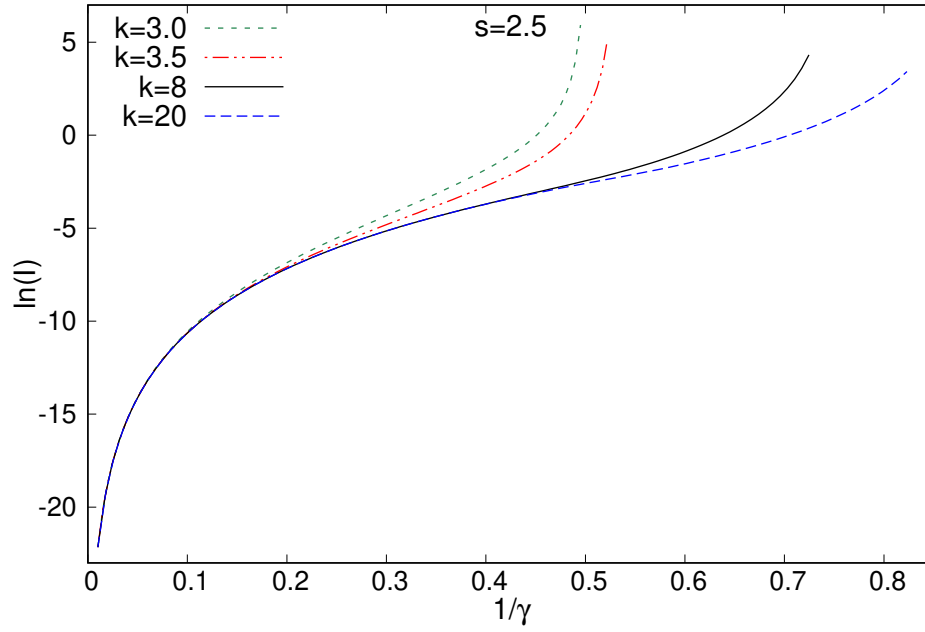


Figure 1: The logarithm of the quantity I , defined in (5.6), against $1/\gamma$, for $s = 2.5$ and $\kappa = 3.0, 3.5, 8, 20$.

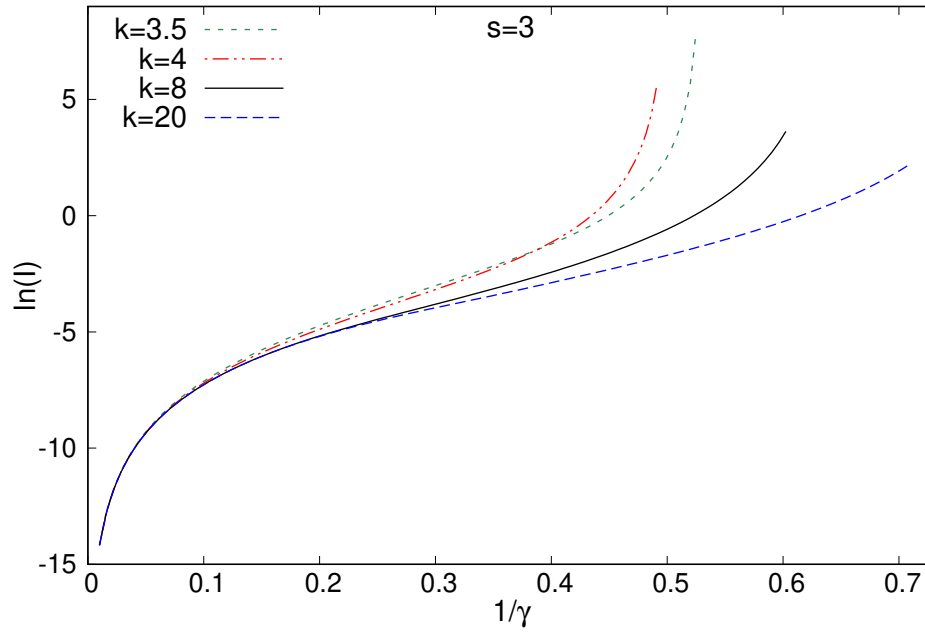


Figure 2: The logarithm of the quantity I , defined in (5.6), against $1/\gamma$, for $s = 3$ and $\kappa = 3.5, 4, 8, 20$.

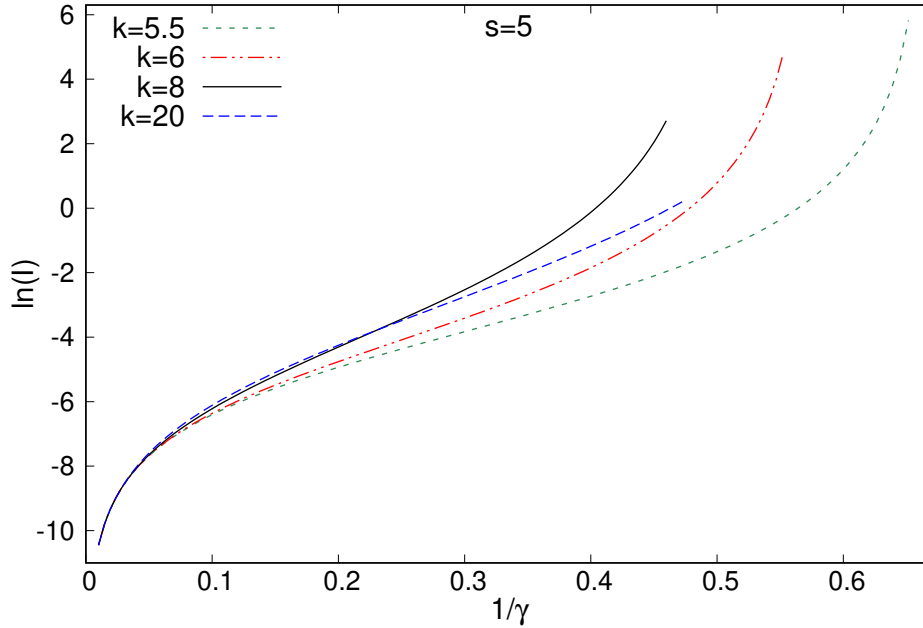


Figure 3: The logarithm of the quantity I , defined in (5.6), against $1/\gamma$, for $s = 5$ and $\kappa = 5.5, 6, 8, 20$.

In Figures 4, 5 and 6, we plot the root-square-mean radius, given in (5.8), in units of $b \equiv \frac{a}{0.524} = \frac{\mu_0}{\beta_2} \frac{1}{\sqrt{2}s 0.524}$, or equivalently $\sqrt{2}s 0.524 \Lambda$, against $I^{1/3}$, with a given in (3.3) and I given in (5.6), for several values of s and κ . Note that the rms radii becomes a linear function of $I^{1/3}$, and so of $|Q|^{1/3}$, very quickly, and as I increases, such linearity reinforces itself. That is in complete agreement with the arguments that we presented in section 3, leading to the relation (3.17). Indeed, as the integration constant γ approaches its critical value $\gamma_{\text{crit.}}$ the rms radii scales as $|Q|^{1/3}$. In order to see that such a thing indeed happens close to $\gamma_{\text{crit.}}$, one should observe that in the three plots in Figures 4, 5 and 6, the linear relation becomes reasonably valid for $I^{1/3} > 0.5$, which corresponds to $\ln(I) > -2.08$. From Figures 1, 2 and 3, one observes that it corresponds to $\gamma < 3.3$, and so reasonably inside the region right above the critical value $\gamma_{\text{crit.}}$, given in (5.11).

Note from Figures 4, 5 and 6 that as $I \rightarrow 0$, and so $\gamma \rightarrow \infty$, the radius goes to a non-zero constant independent of κ . That is the value of the radius we give in (5.14). For $s = 2.5, 3$ and 5 they are respectively $2.6437, 1.8195$ and 0.4949 , in units of $b \equiv \frac{a}{0.524} = \frac{\mu_0}{\beta_2} \frac{1}{\sqrt{2}s 0.524}$, and they correspond to the numerical limit $I \rightarrow 0$ in the Figures 4-6.

Again, all such results are valid for any choice of the coupling constants, as we have not fixed the values of any of them so far. Therefore, the fact that the root-square-mean radius depends linearly upon $|Q|^{1/3}$ is a quite robust property of our model. The choice of s and κ will be used to fix the slope of that linear relation, and so makes it compatible with the experimental data.

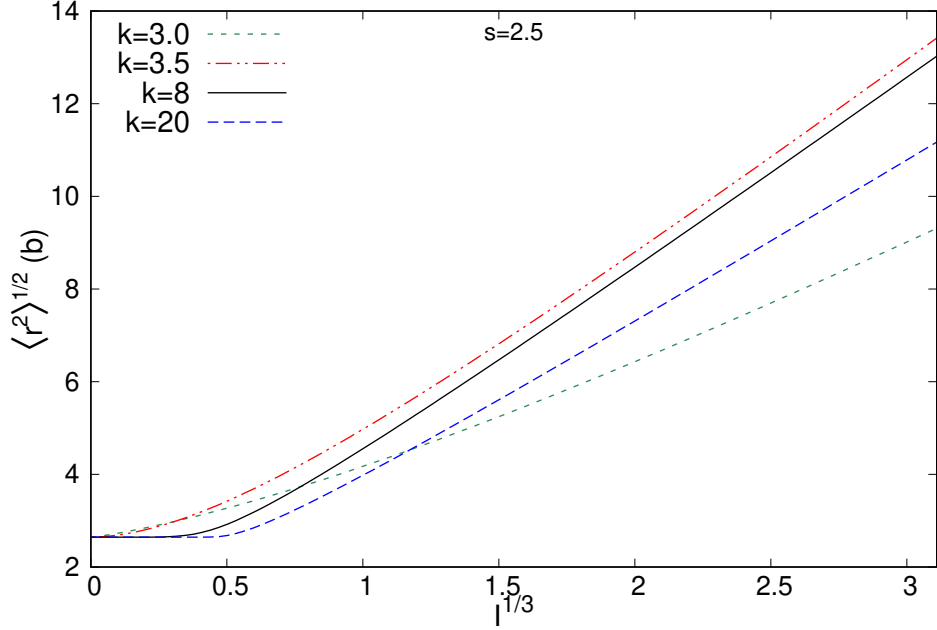


Figure 4: The rms radii (5.8), in units of $b \equiv \frac{a}{0.524} = \frac{\mu_0}{\beta_2} \frac{1}{\sqrt{2} s 0.524}$, with a given in (3.3), against $I^{1/3}$, for $s = 2.5$ and $\kappa = 3.0, 4.5, 8, 20$.

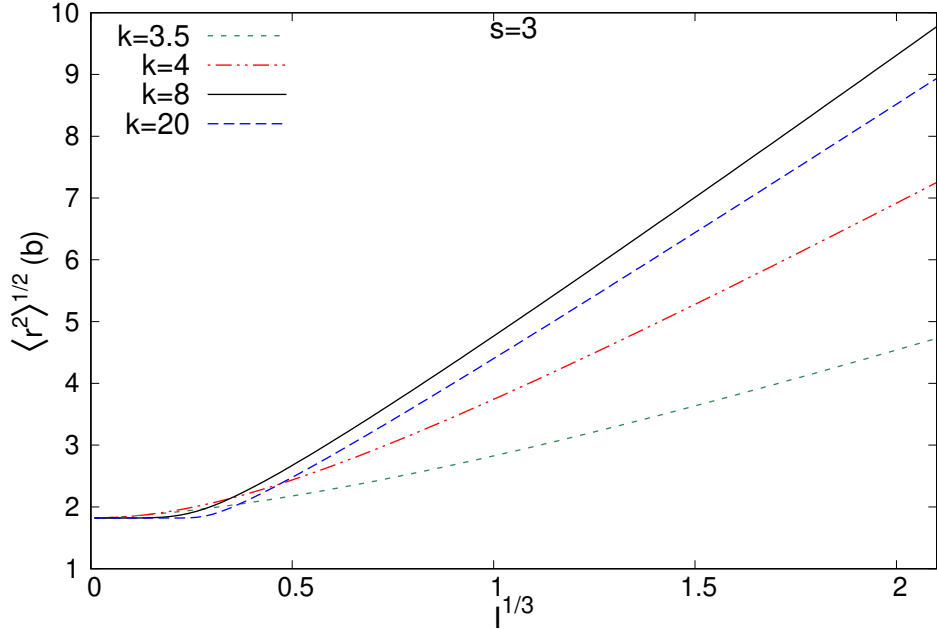


Figure 5: The rms radii (5.8), in units of $b \equiv \frac{a}{0.524} = \frac{\mu_0}{\beta_2} \frac{1}{\sqrt{2} s 0.524}$, with a given in (3.3), against $I^{1/3}$, for $s = 3$ and $\kappa = 3.5, 4, 8, 20$.

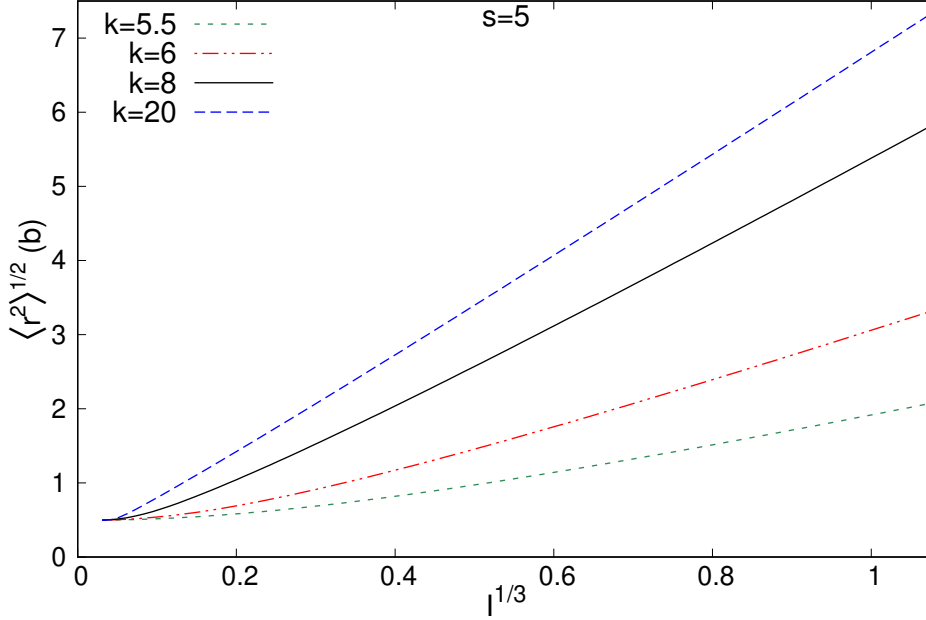


Figure 6: The rms radii (5.8), in units of $b \equiv \frac{a}{0.524} = \frac{\mu_0}{\beta_2} \frac{1}{\sqrt{2} s 0.524}$, with a given in (3.3), against $I^{1/3}$, for $s = 5$ and $\kappa = 5.5, 6, 8, 20$.

5.2 The choice of the functional G and the binding energy per nucleon

Note that if we take G , introduced in (2.10), as a function of $g \equiv (f - \sin f)$, we have that it is a functional of $\text{Tr } U$, and so the symmetry $SU(2)_L \otimes SU(2)_R$ of (2.1) is broken to the diagonal $SU(2)$ subgroup. In addition, using (3.8) we get that

$$\int d^3x G \psi^s = -\frac{2\pi}{(m_0 e_0)^3} [F(g(\infty)) - F(g(0))]; \quad \text{with} \quad \frac{dF}{dg} = G \quad (5.21)$$

From the boundary conditions for f we observe that such a quantity is a functional of $|Q|$. As we have shown in Section 4, if Q is a monotonic function of c , which is supported numerically for plenty of distinct admissible potentials $V_{\text{eff.}}$, then the binding energy per nucleon (4.5) associated with the static energy (2.8) with $G = 0$ is monotonically increasing with Q and saturates at $Q \rightarrow \infty$. As we have argued on the paragraph before (4.11), taking G proportional to $|Q|^2$, it accounts for the Coulomb repulsive interaction of the protons, for the type of nuclei we are considering. So, we choose G as $G = -\beta_G^2 (f - \sin f) / (2\pi)$, and from (2.10) we obtain

$$E_2 = \sigma_2 \left[\vartheta \left(\frac{\mu_0}{\beta_2} \right)^3 \mathcal{E} + \frac{\sigma_G}{2} |Q|^2 \right] \quad (5.22)$$

where

$$\sigma_2 = \frac{4\pi^2 \beta_2^2}{m_0^3 e_0^3} \left(\frac{\beta_\kappa^2}{\beta_2^2} \right)^{\frac{s-2}{\kappa-2}}; \quad \sigma_G = \frac{\beta_G^2}{\beta_2^2} \left(\frac{\beta_2^2}{\beta_\kappa^2} \right)^{\frac{s-2}{\kappa-2}} \quad (5.23)$$

and

$$\mathcal{E} = \frac{1}{\pi} \int_0^\infty d\zeta \zeta^2 \left[\frac{(\hat{\psi}')^2}{2} + \hat{\psi}^2 + \hat{\psi}^\kappa \right] \quad (5.24)$$

So, the binding energy per nucleon (4.5) becomes

$$E_B = \sigma_2 \left[\vartheta \left(\frac{\mu_0}{\beta_2} \right)^3 \left(\mathcal{E}_{Q=1} - \frac{\mathcal{E}}{|Q|} \right) + \frac{\sigma_G}{2} (1 - |Q|) \right] \quad (5.25)$$

6 The data analysis

We consider a list of $N_c = 265$ nuclei, containing all the stable nuclei up to ^{208}Pb , and above that, nuclei up to ^{240}Pu with a half-life greater than 10^3 years, according to [35]. We have a gap in the mass number A from $A = 210$ to $A = 225$, since there are no nuclei matching those criteria of stability and half-life. We shall use the experimental values of charge radii as given by [33], and the values of binding energies per nucleon as given in [34]. The complete list of the 265 nuclei with their experimental radii and binding energies are given in the table of Appendix B.

As we have seen in (3.3), our model predicts that the density of nuclear matter falls to zero, at large distances, with a rate independent of the mass number. That is in good agreement with experimental facts. Indeed, a measure of that is the so-called skin thickness parameter t , which is defined as the distance over which the charge density falls from 90% of its central value to 10%. The value of t is practically independent of the mass number, and it is approximately given by 2.3 Fermi. Using the two-parameter Fermi model for nuclear matter, i.e. $\rho(r) = \rho_0 / (1 + e^{(r-c)/a})$, one gets that $t = a 4 \ln 3$, and so a is approximately equal to 0.524 Fermi. Therefore, from (3.2), (3.3) and (5.2), we shall set

$$a = 0.524 \text{ fm}; \quad \frac{\mu_0}{\beta_2} = s \sqrt{2} 0.524 \text{ fm} \quad (6.1)$$

Then the root-square-mean radius of the baryonic charge, given in (5.8), has its scale fixed, and we are left to choose what value of γ corresponds to a given nuclei. We shall choose ^{56}Fe as the reference nucleus, and so we have $Q(^{56}\text{Fe}) = 56$ and $\sqrt{\langle r^2 \rangle} (^{56}\text{Fe}) = 3.7377 \text{ fm}$, according to [33]. We then find the value of γ corresponding to the reference nucleus ^{56}Fe by solving the following relation, obtained from (5.8),

$$3.7377 \text{ fm} = s \sqrt{2} 0.524 \text{ fm} \sqrt{\frac{J(\gamma(^{56}\text{Fe}), s, \kappa)}{I(\gamma(^{56}\text{Fe}), s, \kappa)}} \quad (6.2)$$

Note that the function $\sqrt{J/I}$ is a monotonic function of γ , and so (6.2) is a well-defined condition for finding $\gamma(^{56}\text{Fe})$.

The value of ϑ is then fixed by the relation (5.5), through

$$56 = s^3 \left(\sqrt{2} 0.524 \text{ fm} \right)^3 \vartheta I(\gamma(^{56}\text{Fe}), s, \kappa) \quad (6.3)$$

Once that is done, we find the discrete sequence of values of γ that lead to integer values of the baryonic charges Q , given by (5.5). With that sequence we can find the rms radii $R \equiv \sqrt{\langle r^2 \rangle}$ for the nuclei corresponding to those values of charge. We have observed that the slope of the curve $R \times Q^{1/3}$ depends stronger on s than on κ , and the best fit to the experimental data corresponds to $s = 3$. We present such result in the Figure 7, and the numerical values of radii are given in the table of Appendix B.

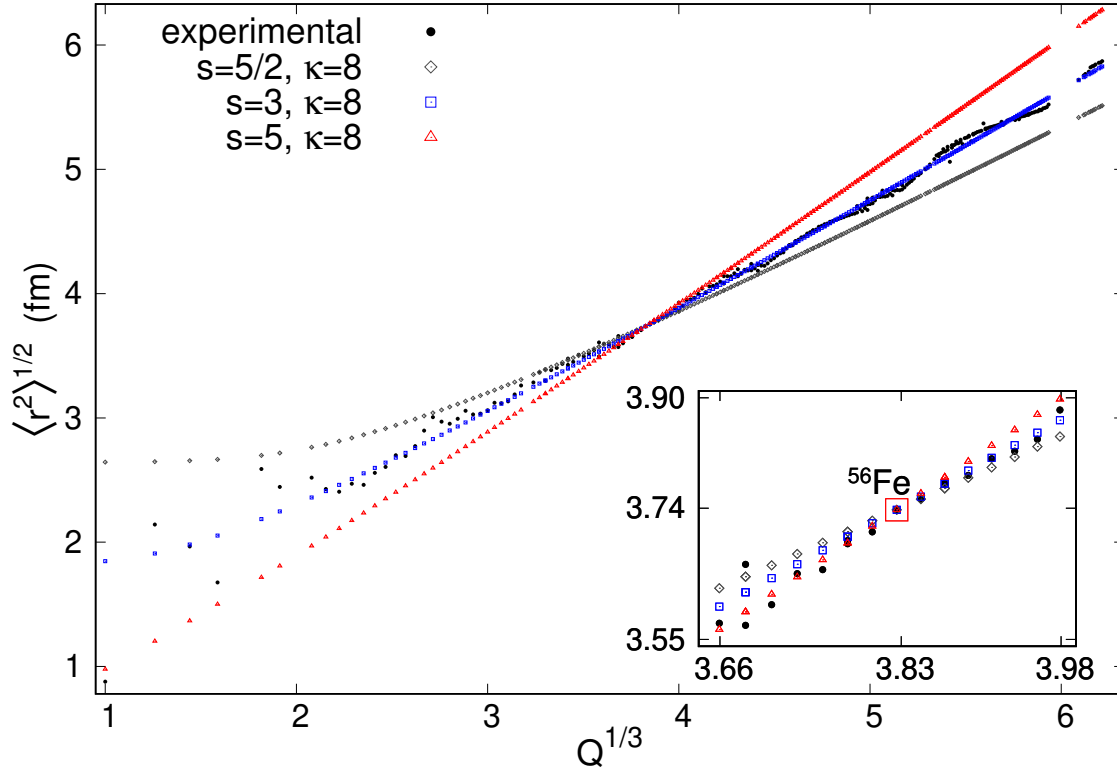


Figure 7: The rms radii $\sqrt{\langle r^2 \rangle}$ as a function of $Q^{1/3}$, with $\kappa = 8$ and $s = 5/2, 3, 5$.

The experimental and the numerical data are compared using the RMSD of the rms radii $R \equiv \sqrt{\langle r^2 \rangle}$ and the binding energy per nucleon E_B , defined respectively by

$$\Delta R = \sum_{\text{list}} \sqrt{\frac{(R^{\text{num.}} - R^{\text{exp.}})^2}{N_c}}; \quad \Delta E_B = \sum_{\text{list}} \sqrt{\frac{(E_B^{\text{num.}} - E_B^{\text{exp.}})^2}{N_c}} \quad (6.4)$$

where the sum in (6.4) is over the entire list of $N_c = 265$ nuclei defined above. The numerical values $R^{\text{num.}}$ and $E_B^{\text{num.}}$ are obtained respectively from (5.8) and (5.25) and the experimental

values $R^{\text{exp.}}$ and $E_B^{\text{exp.}}$ are given respectively in [33] and [34]. We also define $\Delta R^{A \geq 12}$ and $\Delta E_B^{A \geq 12}$ by restricting the sum of (6.4) to $A \geq 12$ and taking $N_c^{A \geq 12} = 256$, where the lightest nucleus is ^{12}C . We have found that, for $s = 3$, ΔR varies from 0.1287 fm for $\kappa = 4$, to 0.0837 fm for $\kappa = 20$, with a very shallow minimum at 0.0820 fm for $\kappa = 8$.

We restrict to the case $s = 3$, $\kappa = 8$, since it gives a very good fit to the radii experimental data. As the values of ϑ and μ_0/β_2 have been fixed already, that also fixes the discrete sequence of values of γ , and so the value of $\mathcal{E}_{Q=1}$ (see (5.24) and (5.25)). Therefore, we look for the values of σ_2 and σ_G , that give the best fit to the experimental values of the binding energies per nucleon as given in [34], and find that

$$\sigma_2 = 2.16499 \text{ MeV}; \quad \sigma_G = 0.00989002; \quad \Delta E_B = 0.216247 \text{ MeV} \quad (6.5)$$

The experimental and theoretical results are shown in Figure 8, and they agree with quite good accuracy (1% or less for $Q > 20$). Once the binding energy is given we can determine the ratio m_0/e_0 from the proton mass, i.e.

$$m_p c^2 = 938.272081 \text{ MeV} = E(Q = 1) = 48 \pi^2 (m_0/e_0) + E_2(Q = 1) \quad (6.6)$$

and so

$$m_0/e_0 = 1.94999 \text{ MeV} \quad (6.7)$$

Then, all parameters of our model are fixed except for the ratio β_κ/β_2 . So, the original parameters of the model become

$$\begin{aligned} m_0^2/\alpha &= 4.40047 \text{ MeV/fm}; & e_0^2/\alpha &= 1.15727 \text{ MeV}^{-1} \text{ fm}^{-1} \\ \mu_0^2/\alpha^2 &= 3.11483 \text{ MeV/fm}; & \beta_2^2/\alpha^2 &= 0.63023 \text{ MeV/fm}^3 \\ \beta_G^2/\alpha^3 &= 0.00623 \text{ MeV/fm}^3; & \text{with } \alpha &= (\beta_\kappa/\beta_2)^{\frac{1}{3}} \end{aligned} \quad (6.8)$$

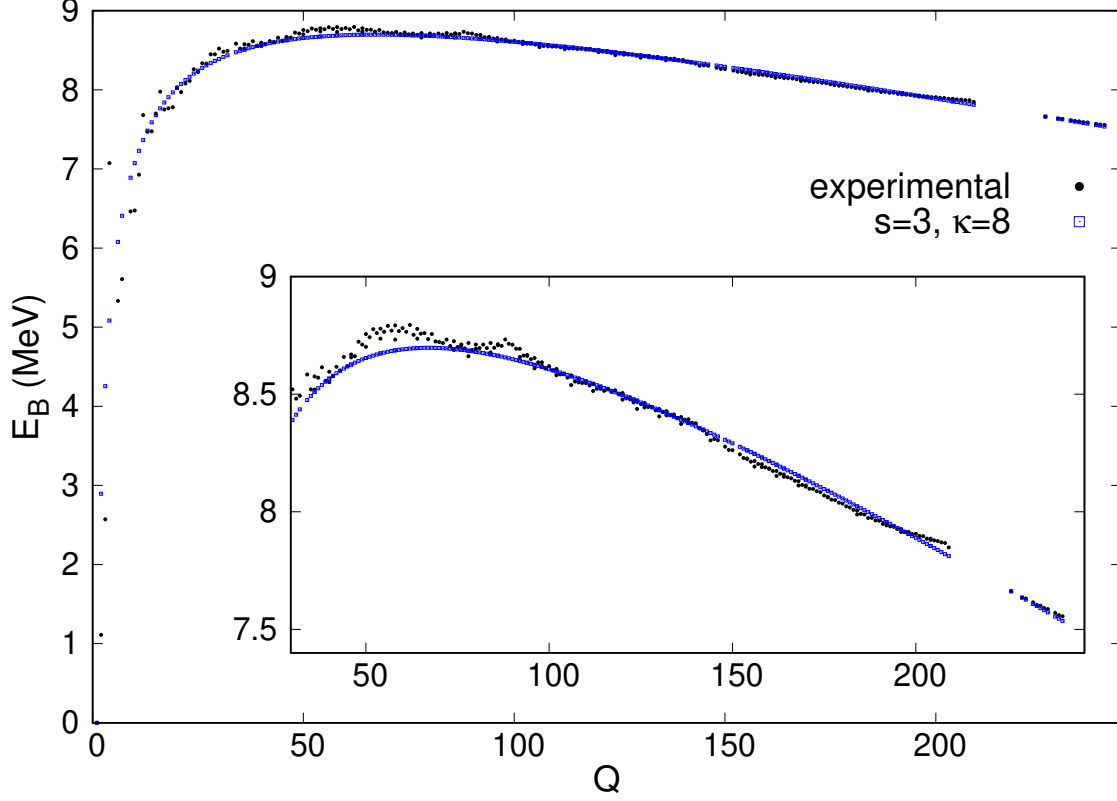


Figure 8: The binding energy per nucleon E_B , as a function of Q , for $\kappa = 8$ and $s = 3$, and the best fit corresponding to $\sigma_2 = 2.16499 \text{ MeV}$, $\sigma_G = 0.00989002$ where the RMSD is $\Delta E_B = 0.216247 \text{ MeV}$.

In Figure 9 we plot the density of the baryonic charge as given by (5.7), in units of fm^{-3} , as a function of the radial distance r , in units of fm , for several values of the baryonic charge. Note that the value of the density at the origin increases up to $Q = 17$, and then it decreases slowly to 0.1645 fm^{-3} , for $Q = 240$, and that is very close to the experimental values for heavy nuclei given in many text books. The PREX Collaboration has recently obtained that the interior baryon density of the nucleus ^{208}Pb is $0.1480 \pm 0.0038 \text{ fm}^{-3}$ [43].

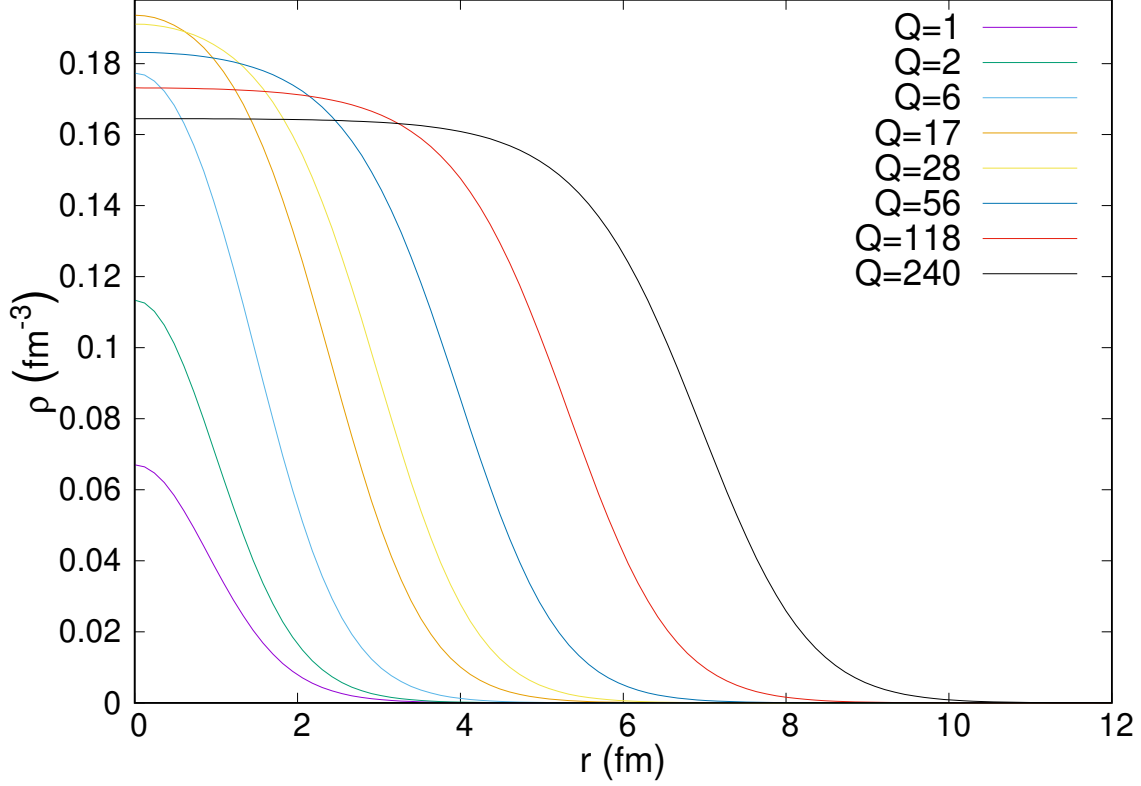


Figure 9: The topological charge density $\rho = \frac{\vartheta}{4\pi^2} \hat{\psi}^s (\zeta = r / (s \sqrt{2} 0.524 \text{ fm}))$ corresponding to the numerical solutions shown in Figure 7, for the parameters $\kappa = 8$ and $s = 3$. Note that the value of $\rho(r = 0)$ increases up to $Q = 17$ and then decreases slowly to about 0.1645 fm^{-3} for $Q = 240$.

In Figure 10 we show how the value of $\hat{\psi}$ at the origin, i.e. $\hat{\psi}(\zeta = 0)$, varies with the quantity $I^{1/3}$, with I defined in (5.6). Note that according to (5.5), I is proportional to the baryonic charge. From (5.7) we have that the baryonic charge density at the origin is $\rho(0) = \frac{\vartheta}{4\pi^2} \hat{\psi}^s(0)$. The value of the integration constant γ decreases as we move along the curves from left to right. We observe that, as γ decreases, $\hat{\psi}(0)$ increases up to a maximum and then decreases, approaching a constant value as γ goes to its critical value (see (5.11)). However, the plots in Figure 10 end before γ reaches its critical value. For $s = 3$ and $\kappa = 3.5, 4, 8$ the lowest values of γ are respectively 1.905, 2.025, 1.660. In the zoomed plot in Figure 10 we show, for $s = 3$ and $\kappa = 8$, the values of $\hat{\psi}(0)$ for $Q = 1, 56$ and 240 , for the choice of ^{56}Fe as the reference nucleus (see (6.3)).

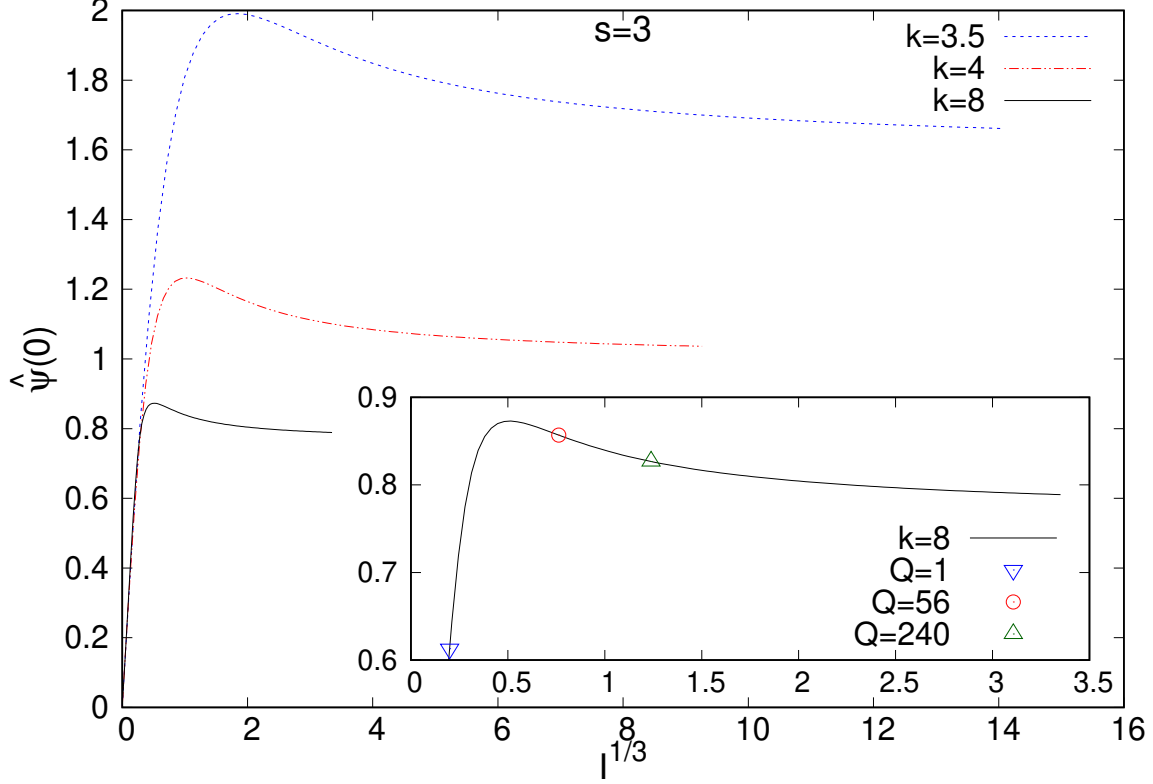


Figure 10: The value of the solution of (5.4) at the origin, i.e. $\hat{\psi}(0)$, against $I^{1/3}$ for $s = 3$ and $\kappa = 3.5, 4, 8$. In the zoomed plot we show the values of $\hat{\psi}(0)$ for the values of baryonic charge $Q = 1, 56, 240$, for the particular choice of ^{56}Fe as the reference nuclei and the value of the ratio μ_0/β_2 fixed by (6.1). The integration constant γ decreases from the left to the right, with its highest value being 100. For $\kappa = 3.5, 4, 8$ the lowest values of γ are respectively 1.905, 2.025, 1.660.

The Table 1 below shows that the models corresponding to $s = 3$ and $\kappa = 6, \dots, 20$ are in good agreement with the experimental data for both R and E_B , specially for $A \geq 12$ where the RMSD of $\sqrt{\langle r^2 \rangle}$ drops to about half and the RMSD of E_B drops to about a quarter. The rms radii experimental data [33] for the list of 265 nuclei defined above, can be fitted by

$$\begin{aligned} \sqrt{\langle r^2 \rangle}_{exp.} &= (0.56386 + 0.839967 Q^{1/3}) \text{ fm} \\ \sqrt{\langle r^2 \rangle}_{exp.}^{A \geq 12} &= (0.50530 + 0.85156 Q^{1/3}) \text{ fm} \end{aligned} \quad (6.9)$$

and the RMSD are respectively 0.07555 fm and 0.03789 fm , which are close to the values of ΔR and $\Delta R^{A \geq 12}$ for $s = 3$ and $\kappa \geq 6$, shown in Table 1 below. Note the smooth variation of $\Delta R_{s=3}$ and $\Delta R_{s=3}^{A \geq 12}$ for $\kappa \geq 6$, being respectively about 3.0% and 7.5% as compared to its maximum value at $\kappa = 6$. Note also that $\Delta E_{B,s=3}$ monotonically decreases from its maximum value at $\kappa = 7$ to its minimum value at $\kappa = 20$. The situation reverses for

the case of $\Delta E_{B,s=3}^{A \geq 12}$ which is monotonically increasing for all κ . For $s = 3$ the maximum variation of ΔR , $\Delta R^{A \geq 12}$, ΔE_B and $\Delta E_B^{A \geq 12}$ in relation to its maximum for all values of κ are respectively 36.3 %, 60.0 %, 0.5 %, 1.3 %.

Table 1: The RMSD ΔR (fm) of the rms radii and $\Delta R^{A \geq 12}$ (fm) for any the integer value of $\kappa > s$ up to $\kappa = 20$ and for $s = 5/2, 3, 5$ and for $s = 3$. We also give the RMSD of the binding energy per nucleon ΔE_B (MeV) and $\Delta E_B^{A \geq 12}$ (MeV).

κ	$\Delta R_{s=5}$	$\Delta R_{s=5}^{A \geq 12}$	$\Delta R_{s=5/2}$	$\Delta R_{s=5/2}^{A \geq 12}$	$\Delta R_{s=3}$	$\Delta R_{s=3}^{A \geq 12}$	$\Delta E_{B,s=3}$	$\Delta E_{B,s=3}^{A \geq 12}$
3	*	*	0.63344	0.61523	*	*	*	*
4	*	*	0.41324	0.38721	0.12874	0.10108	0.215518	0.047759
5	*	*	0.31961	0.28696	0.09332	0.05644	0.216087	0.047923
6	0.33417	0.31942	0.27335	0.23556	0.08454	0.04373	0.216271	0.048066
7	0.29802	0.28192	0.24750	0.20578	0.08241	0.04077	0.216295	0.048156
8	0.27233	0.25519	0.23165	0.18693	0.08204	0.04047	0.216247	0.048213
9	0.25317	0.23518	0.22123	0.17421	0.08216	0.04079	0.216166	0.048250
10	0.23834	0.21964	0.21401	0.16519	0.08239	0.04118	0.216071	0.048275
11	0.22654	0.20723	0.20878	0.15853	0.08263	0.04151	0.215972	0.048292
12	0.21693	0.19709	0.20487	0.15347	0.08284	0.04177	0.215873	0.048306
13	0.20896	0.18864	0.20185	0.14952	0.08302	0.04196	0.215777	0.048317
14	0.20225	0.18150	0.19948	0.14638	0.08317	0.04211	0.215686	0.048326
15	0.19652	0.17538	0.19757	0.14383	0.08330	0.04221	0.215600	0.048334
16	0.19157	0.17009	0.19601	0.14173	0.08341	0.04229	0.215520	0.048342
17	0.18726	0.16546	0.19472	0.13998	0.08350	0.04234	0.215445	0.048349
18	0.18346	0.16137	0.19364	0.13850	0.08357	0.04238	0.215375	0.048355
19	0.18010	0.15774	0.19272	0.13724	0.08364	0.04241	0.215310	0.048362
20	0.17711	0.15450	0.19193	0.13616	0.08369	0.04243	0.215249	0.048368

6.1 The influence of the reference nucleus on the data analysis

We have seen that the integration constant γ plays the role of a running coupling constant, in the sense that as we vary it, all the relevant quantities associated to the solution, including the quantity I defined in (5.6), also vary. In fact, in Figures 1, 2 and 3 we have shown that I , and consequently the baryonic charge Q (see (5.5)), are monotonically decreasing functions of γ . In order to find what value of γ corresponds to a given value of Q , we have to choose a reference nucleus and use some of its experimental data to fix the scales.

In (6.1) the value of the ratio of coupling constants μ_0/β_2 was fixed by choosing the value of the parameter a that gives the rate of the fallout of the solution at large distances. Then choosing ^{56}Fe as the reference nucleus, and using the experimental value of its rms charge

radius, we found the value of γ corresponding to ^{56}Fe through (6.2). Then the value of the coupling constant ϑ was fixed through (6.3). Once that is done the discrete sequence of values of γ corresponding to all the other nuclei are found, using (5.5), through

$$Q = \frac{Q_{\text{ref.}}}{I_{\text{ref.}}} I \quad (6.10)$$

where $Q_{\text{ref.}}$ is the baryonic charge of the reference nucleus, and $I_{\text{ref.}} = I(\gamma_{\text{ref.}}, s, \kappa)$, with $\gamma_{\text{ref.}}$ being the value of γ found through (6.2).

The question is how our data analysis is affected by the change of the reference nucleus. Clearly, if the ratio $\frac{Q_{\text{ref.}}}{I_{\text{ref.}}}$ is not affected much by such a change, nothing will be drastically modified. Indeed, the value of I corresponding to a given Q will change little, and so it will not change drastically the value of γ associated to that same Q , since I is a monotonic (decreasing) function of γ .

In order to give some examples, let us fix μ_0/β_2 as in (6.1). The choice of ^{56}Fe as the reference nucleus leads to a RMSD of the radii of 0.00820 fm and $I(\gamma(^{56}\text{Fe}), \kappa = 8, s = 3)/56 = 0.0079194$. If we take instead ^{108}Pd as the reference nucleus we get a very similar ratio, i.e. $I(\gamma(^{108}\text{Pd}), \kappa = 8, s = 3)/108 = 0.0080002$, and as expected we obtain a similar RMSD of the radii given by 0.08225 fm . Taking the reference nucleus as any of the nuclei with $Q > 50$ in our list defined at the beginning of section 6, the ratio $I(\gamma_{\text{ref.}}, \kappa = 8, s = 3)/Q_{\text{ref.}}$ oscillates between a minimum of 0.0075710 at ^{86}Kr and a maximum of 0.0084839 at ^{78}Kr . In Figure 11 we plot the ratio $I(\gamma_{\text{ref.}}, \kappa = 8, s = 3)/Q_{\text{ref.}}$ against Q , by taking each one of the 265 nuclei in our list mentioned above, as the reference nucleus. Therefore, we should not expected a drastic change in the plots of Figures 7 and 8 for the radii and binding energies, by replacing ^{56}Fe by another heavy reference nucleus in our list. The only restriction we have is the following. As we have seen in (5.14), and also in the Figures 4, 5 and 6, our model presents a lower bound for the radius for $\gamma \rightarrow \infty$. Therefore, a restriction on the choice of the reference nucleus is that it can not have an experimental rms radius R^{exp} lower than that bound. Using (6.1) for $s = 3$ we get from (5.14) that $\sqrt{\langle r^2 \rangle}_{\text{min.}} = 1.8195 \text{ fm}$, and so we cannot take as the reference nucleus only ^1H and ^3He in our list of $N_c = 265$ nuclei defined at the beginning of section 6.

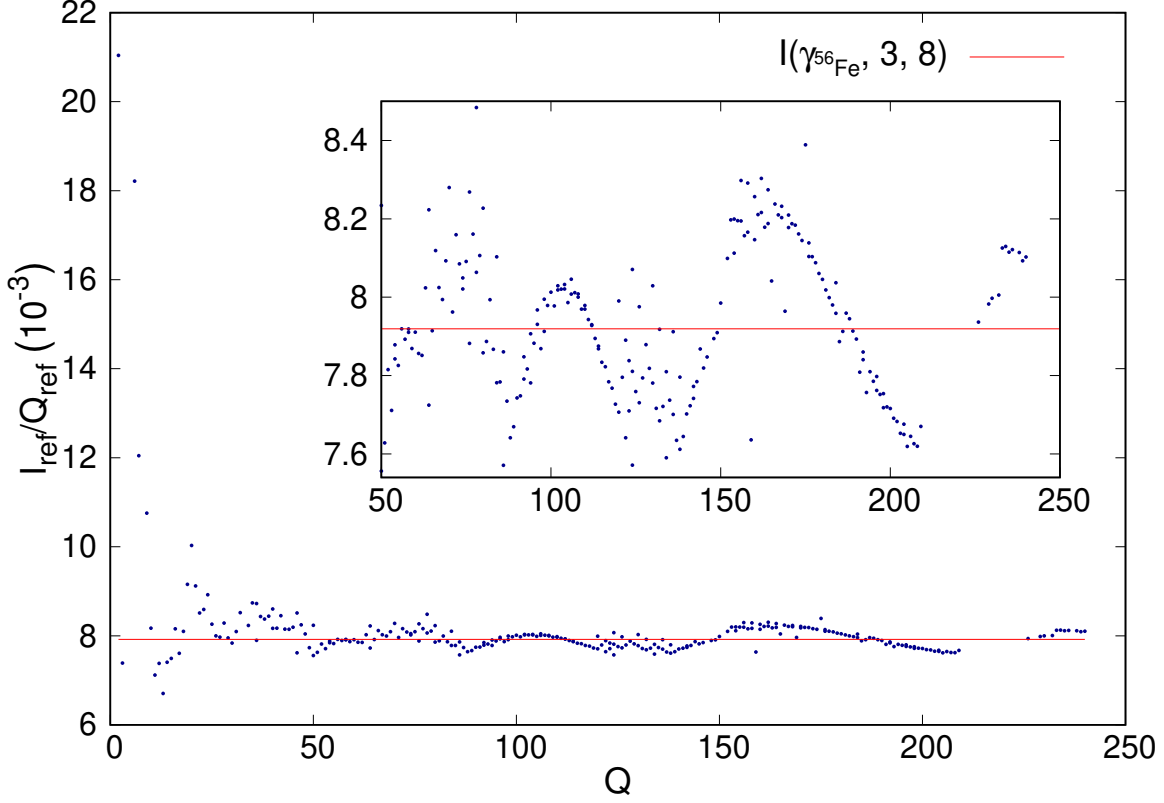


Figure 11: The $I_{\text{ref.}}(\gamma_{\text{ref.}}, s, \kappa)/Q_{\text{ref.}}$ corresponding to taking each nuclei in our list as the referential nuclei vs. Q for $s = 3$ and $\kappa = 8$, but without distinguishing the isotopes.

For $s = 3$, and $\kappa = 4, \dots, 14$, we have evaluated the radii RMSD for every choice of the reference nucleus in our list, except for the ^1H and $^3\text{He}^3$. We have obtained the values of κ that gives the lowest values of ΔR and $\Delta R^{A \geq 12}$, as defined in (6.4). Such RMSD values are plotted in the Figure 12, without distinguishing the isotopes, and we see that it does not change drastically for non-light nuclei. So our data analysis should not change much by the replacement of the reference nucleus. In addition, we obtain that:

1. The smallest ΔR occurs for ^{18}O at $\kappa = 7$ where $\Delta R = 0.0818 \text{ fm}$ and $\Delta R^{A \geq 12} = 0.0395 \text{ fm}$.
2. The smallest $\Delta R^{A \geq 12}$ occurs for ^{68}Zn at $\kappa = 6$ where $\Delta R = 0.0825 \text{ fm}$ and $\Delta R^{A \geq 12} = 0.0394 \text{ fm}$.

³The step size of the Runge-Kutta was reduced to $h = 0.005$.

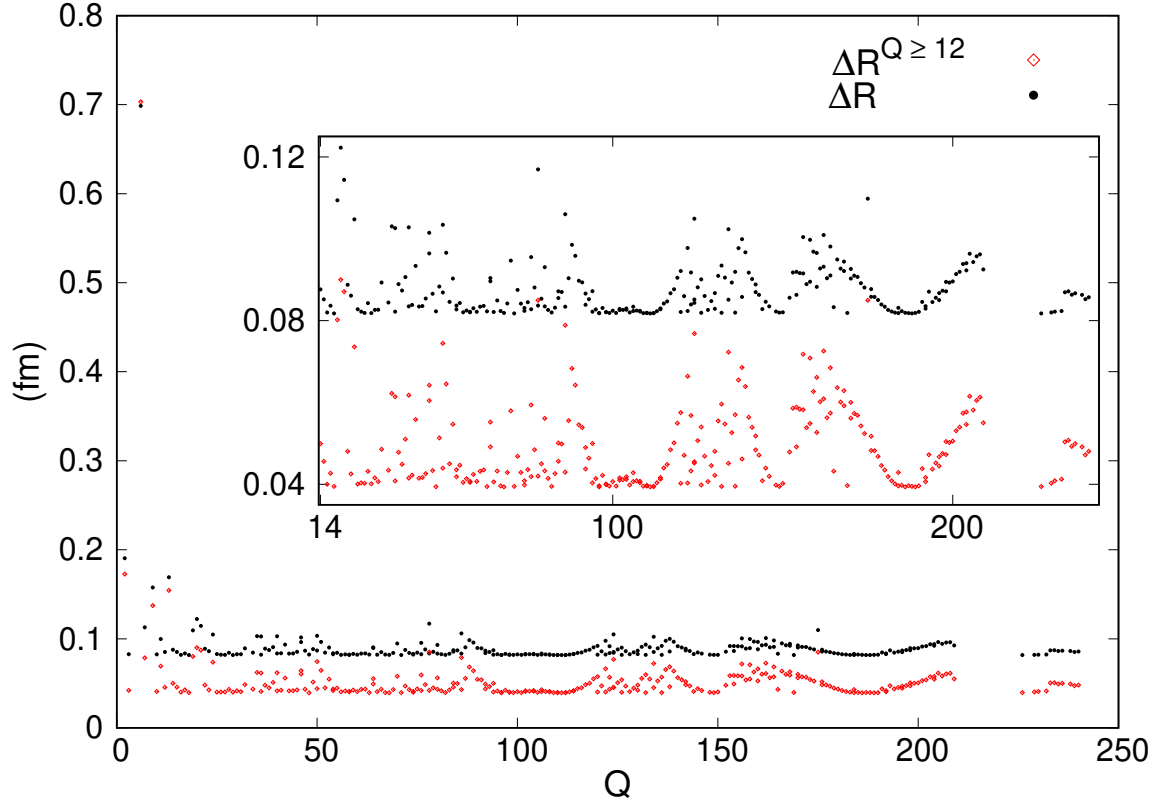


Figure 12: The smallest ΔR and $\Delta R^{A \geq 12}$ for $s = 3$ among all values of $\kappa = 4, \dots, 15$ for each choice of the reference nucleus in our list, defined at the beginning of section 6, excluding ${}^1\text{H}$ and ${}^4\text{He}$.

7 Conclusion

The Skyrme-type model presented in this paper reproduces with quite good accuracy, in a simple and robust way, some bulk properties of nuclei, like the radii and the binding energies, for a very wide range of values of the mass number. It is a very good improvement as compared to the results obtained by other modifications of the Skyrme model, and may be of interest for applications in other areas of physics too.

Our results are better for heavier nuclei than for light ones, and that is expectable since our density of baryonic charge is spherically symmetric mainly due to Coleman's false vacuum arguments. One could improve on that in several ways, including the consideration of other potentials. However, we have observed that the RMSD for radii and binding energies are insensitive to κ as long as $s = 3$ and $\kappa \geq 6$. We believe that the first improvement of the model should involve the breaking of the self-duality, which could be achieved by introducing h -dependent terms like kinetic and potential energies for the h -fields. That modification of the model has to be small and could perhaps be treated by a perturbation theory. It could lead to non-spherically symmetric solutions and perhaps to a better description of light nuclei.

Another line to be pursued is the study of time dependent (spinning) solutions, that could break even more the symmetries, as for instance the degeneracy between protons and neutrons, and enrich the spectrum of the model. In order to do that one needs an action in Minkowski space-time. The action corresponding to E_1 is given in [32, 36], and a possible action associated to E_2 is

$$S_2 = \int d^4x \left[\frac{\mu_0^2}{4s^2} K^{-2(1-1/s)} C_{\mu\nu}^2 - V(K) + G(U) K \right] \quad (7.1)$$

with

$$B_\mu = -\frac{i}{12\lambda^3} \varepsilon_{\mu\nu\rho\sigma} \widehat{\text{Tr}}(R^\nu R^\rho R^\sigma); \quad C_{\mu\nu} = \partial_\mu B_\nu - \partial_\nu B_\mu; \quad K = \sqrt{B_\mu B^\mu} \quad (7.2)$$

Of course that should be considered as a low energy effective action, and one should restrict to low frequencies where $B_0^2 > B_i^2$.

But the most interesting question to address is that of the nature of such a model. Since it reproduces some bulk properties of nuclei, it would be interesting to investigate if it could give some insights into the strong coupled regime of the strong interactions and if it connects to some low energy limit of QCD.

Acknowledgements: LAF is partially supported by Conselho Nacional de Desenvolvimento Científico e Tecnológico - CNPq (contract 308894/2018-9), and LRL is supported by a CAPES scholarship.

A The numerical methods

The solutions of the ordinary differential equation (5.4), satisfying $\hat{\psi}'(0) = 0$ and $\hat{\psi}(\infty) = \hat{\psi}'(\infty) = 0$, were obtained, for each value of κ and s , using the fourth-order explicit Runge-Kutta method with the step size $\Delta\zeta = 10^{-4}$, and ζ lying in the finite interval $[0, \zeta_{\max}]$. The value of ζ_{\max} , and so the size of the adaptive lattice, is the maximum value of ζ such that $0 < \hat{\psi}(\zeta_{\max.}) < 1.2 \times 10^{-5}$, $\hat{\psi}(\zeta_{\max.})' < 0$ and $|\hat{\psi}'(\zeta_{\max.})| < 10^{-8}$. We use the shooting method by varying the value of $\hat{\psi}(0)$, and our final numerical solution will be an undershoot configuration approximating the bounce solution in the finite interval given above, such that any increment of 10^{-14} in $\hat{\psi}(0)$ gives an overshoot configuration. Typically we have $\zeta_{\max.} \sim 10 - 20$.

The discrete sequence of values of γ corresponding to integer values of the baryonic charge Q is found in two steps. First, we obtain the value of $\gamma(^{56}\text{Fe})$ successively solving the equation (5.4) by varying γ using unbounded binary search until $\sqrt{J/I}$ differs from its value given by the relation (6.2), by less than 10^{-10} , where $3.7377 fm$ is the value of the rms radius of the nucleus ^{56}Fe , according to [33]. The value of ϑ is fixed through the equation (6.3).

Second, we do the same to find the discrete sequence of γ corresponding to the integer values of the Skyrme charges Q , given by (5.5), where the ratio $\frac{\mu_0}{\beta_2}$ is fixed through (6.1), which can be rewritten as

$$Q = \frac{I(\gamma, s, \kappa)}{I(\gamma(^{56}\text{Fe}), s, \kappa)/56} \quad (\text{A.1})$$

such that any of its numerical value $Q_{\text{num.}}$ differs from the nearest integer value of Q by $|(Q - Q_{\text{num.}})/Q| < 2 \times 10^{-8}$.

Once this two steps are done, the bounce solution $\hat{\psi}(\zeta)$ is fixed for each value of Q , and so the corresponding Skyrme charge density ρ is determined by (5.7).

B The experimental and numerical data

In the Table 2 below, we provide the experimental and numerical data used in the plots of Figures 7 and 8. A is the mass number and Z is the number of protons of the nucleus. $R^{\text{exp.}}$ stands for the experimental values of the rms charge radii as given in reference [33], and $E_B^{\text{exp.}}$ stands for the experimental values of the binding energy per nucleon as given in [34]. We also provide the numerical results (with the same number of digits as the experimental data) obtained from our model for the case $s = 3$ and $\kappa = 8$. $R^{\text{num.}}$ stands for the numerical rms radii, and $E_B^{\text{num.}}$ for the numerical binding energy per nucleon. We also give the values of the parameter γ for each value of A , i.e. those that lead to an integer value of the topological charge. Since there is more than one stable nucleus for some values of A , but there is only one solution for each Skyrme charge Q , we repeat the numerical values in those cases for easy comparison.

Table 2: The experimental data $R^{\text{exp.}}(fm)$ and $E_B^{\text{exp.}}(MeV)$ and the numerical values $R^{\text{num.}}(fm)$, $E_B^{\text{num.}}(MeV)$ and γ (dimensionless) obtained from our model for the case $s = 3$ and $\kappa = 8$.

Name	A	Z	$R^{\text{exp.}}$	$R^{\text{num.}}$	$E_B^{\text{exp.}}$	$E_B^{\text{num.}}$	γ
H	1	1	0.8783	1.8467	0.000000	0.000000	4.491068461142762
H	2	1	2.1421	1.9087	1.112283	2.895106	3.649869712047377
He	3	2	1.9661	1.9808	2.572680	4.254723	3.275512965240602
He	4	2	1.6755	2.0527	7.073915	5.084109	3.055186690308611
Li	6	3	2.5890	2.1862	5.332331	6.078895	2.797917904594600
Li	7	3	2.4440	2.2473	5.606439	6.407667	2.714002952968850
Be	9	4	2.5190	2.3598	6.462668	6.889732	2.591114911251203
B	10	5	2.4277	2.4117	6.475083	7.072907	2.544219486469452
B	11	5	2.4060	2.4613	6.927732	7.229382	2.503942224117655
C	12	6	2.4702	2.5086	7.680144	7.364775	2.468850343952055
C	13	6	2.4614	2.5540	7.469849	7.483176	2.437910925143941
N	14	7	2.5582	2.5976	7.475614	7.587648	2.410358116708282
N	15	7	2.6058	2.6397	7.699460	7.680532	2.385610494137132
O	16	8	2.6991	2.6802	7.976206	7.763651	2.363217640071331
O	17	8	2.6932	2.7194	7.750728	7.838453	2.342824482983545
O	18	8	2.7726	2.7574	7.767097	7.906102	2.324146819327975
F	19	9	2.8976	2.7942	7.779018	7.967544	2.306954100038247
Ne	20	10	3.0055	2.8300	8.032240	8.023561	2.291057065022768
Ne	21	10	2.9695	2.8648	7.971713	8.074802	2.276298691132936
Ne	22	10	2.9525	2.8986	8.080465	8.121814	2.262547453280112
Na	23	11	2.9936	2.9316	8.111493	8.165058	2.249692231249988
Mg	24	12	3.0570	2.9638	8.260709	8.204929	2.237638407479905
Mg	25	12	3.0284	2.9952	8.223502	8.241766	2.226304840103443
Mg	26	12	3.0337	3.0259	8.333870	8.275862	2.215621488325438
Al	27	13	3.0610	3.0560	8.331553	8.307472	2.205527530232682
Si	28	14	3.1224	3.0854	8.447744	8.336819	2.195969856721151
Si	29	14	3.1176	3.1141	8.448635	8.364099	2.186901855810426
Si	30	14	3.1336	3.1424	8.520654	8.389484	2.178282423400496
P	31	15	3.1889	3.1700	8.481167	8.413128	2.170075152240669
S	32	16	3.2611	3.1972	8.493129	8.435168	2.162247662359158
S	34	16	3.2847	3.2500	8.583498	8.474908	2.147619395869828
Cl	35	17	3.3654	3.2758	8.520278	8.492817	2.140769427267332
S	36	16	3.2985	3.3011	8.575389	8.509539	2.134200134292854
Ar	36	18	3.3905	3.3011	8.519909	8.509539	2.134200134292854
Cl	37	17	3.3840	3.3260	8.570281	8.525155	2.127892515622490
Ar	38	18	3.4028	3.3505	8.614280	8.539738	2.121829333480677
K	39	19	3.4349	3.3746	8.557025	8.553355	2.115994908123602

Continued on next page

Table 2 – *Continued from previous page*

Name	A	Z	$R^{\text{exp.}}$	$R^{\text{num.}}$	$E_B^{\text{exp.}}$	$E_B^{\text{num.}}$	γ
Ca	40	20	3.4776	3.3983	8.551303	8.566065	2.110374940891559
Ar	40	18	3.4274	3.3983	8.595259	8.566065	2.110374940891559
K	41	19	3.4518	3.4217	8.576072	8.577924	2.104956361248827
Ca	42	20	3.5081	3.4448	8.616563	8.588984	2.099727194058634
Ca	43	20	3.4954	3.4675	8.600663	8.599289	2.0946764444000906
Ca	44	20	3.5179	3.4899	8.658175	8.608884	2.089793994574852
Sc	45	21	3.5459	3.5120	8.618931	8.617808	2.085070519558121
Ca	46	20	3.4953	3.5338	8.66898	8.62610	2.080497405145488
Ti	46	22	3.6070	3.5338	8.656451	8.626097	2.080497405145488
Ti	47	22	3.5962	3.5554	8.661227	8.633785	2.076066681276107
Ti	48	22	3.5921	3.5766	8.723006	8.640903	2.071770960893693
Ti	49	22	3.5733	3.5976	8.711157	8.647481	2.067603386077977
Ti	50	22	3.5704	3.6183	8.755718	8.653545	2.063557580146583
Cr	50	24	3.6588	3.6183	8.701032	8.653545	2.063557580146583
V	51	23	3.6002	3.6388	8.742099	8.659121	2.059627604959952
Cr	52	24	3.6452	3.6590	8.775989	8.664232	2.055807922773732
Cr	53	24	3.6511	3.6790	8.760198	8.668900	2.052093362076591
Cr	54	24	3.6885	3.6988	8.777955	8.673146	2.048479086930095
Fe	54	26	3.6933	3.6988	8.736382	8.673146	2.048479086930095
Mn	55	25	3.7057	3.7184	8.765022	8.676988	2.044960569393613
Fe	56	26	3.7377	3.7377	8.790354	8.680445	2.041533564673800
Fe	57	26	3.7532	3.7568	8.770279	8.683533	2.038194088685605
Fe	58	26	3.7745	3.7758	8.792250	8.686269	2.034938397753139
Ni	58	28	3.7757	3.7758	8.732059	8.686269	2.034938397753139
Co	59	27	3.7875	3.7945	8.768035	8.688667	2.031762970212437
Ni	60	28	3.8118	3.8130	8.780774	8.690741	2.028664489709483
Ni	61	28	3.8225	3.8314	8.765025	8.692506	2.025639830011463
Ni	62	28	3.8399	3.8495	8.794553	8.693972	2.022686041171518
Cu	63	29	3.8823	3.8675	8.752138	8.695152	2.019800336906873
Ni	64	28	3.8572	3.8853	8.777461	8.696057	2.016980083066171
Zn	64	30	3.9283	3.8853	8.735905	8.696057	2.016980083066171
Cu	65	29	3.9022	3.9029	8.757096	8.696698	2.014222787076635
Zn	66	30	3.9491	3.9204	8.759632	8.697084	2.011526088274126
Zn	67	30	3.9530	3.9377	8.734152	8.697226	2.008887749029717
Zn	68	30	3.9658	3.9549	8.755680	8.697131	2.006305646596767
Ga	69	31	3.9973	3.9719	8.724579	8.696810	2.003777765609718
Ge	70	32	4.0414	3.9887	8.721700	8.696268	2.001302191174485
Ga	71	31	4.0118	4.0054	8.717604	8.695516	1.998877102495371
Ge	72	32	4.0576	4.0220	8.731745	8.694559	1.996500766990397
Ge	73	32	4.0632	4.0384	8.705049	8.693404	1.994171534851110
Ge	74	32	4.0742	4.0547	8.725200	8.692059	1.991887834007733

Continued on next page

Table 2 – *Continued from previous page*

Name	A	Z	$R^{\text{exp.}}$	$R^{\text{num.}}$	$E_B^{\text{exp.}}$	$E_B^{\text{num.}}$	γ
Se	74	34	4.0700	4.0547	8.687715	8.692059	1.991887834007733
As	75	33	4.0968	4.0708	8.700874	8.690530	1.989648165464452
Se	76	34	4.1395	4.0868	8.711477	8.688822	1.987451098972989
Ge	76	32	4.0811	4.0868	8.705236	8.688822	1.987451098972989
Se	77	34	4.1395	4.1027	8.694690	8.686942	1.985295269015788
Se	78	34	4.1406	4.1184	8.717806	8.684895	1.983179371073147
Kr	78	36	4.2038	4.1184	8.661238	8.684895	1.983179371073147
Br	79	35	4.1629	4.1341	8.687594	8.682686	1.981102158150497
Kr	80	36	4.1970	4.1496	8.692928	8.680320	1.979062437544858
Se	80	34	4.1400	4.1496	8.710813	8.680320	1.979062437544858
Br	81	35	4.1599	4.1650	8.695946	8.677802	1.977059067831450
Kr	82	36	4.1919	4.1802	8.710675	8.675137	1.975090956052185
Kr	83	36	4.1871	4.1954	8.695729	8.672330	1.973157055091182
Kr	84	36	4.1884	4.2104	8.717446	8.669383	1.971256361222048
Sr	84	38	4.2394	4.2104	8.677512	8.669383	1.971256361222048
Rb	85	37	4.2036	4.2253	8.697441	8.666302	1.969387911814059
Kr	86	36	4.1835	4.2402	8.712029	8.663091	1.967550783185259
Sr	86	38	4.2307	4.2402	8.708456	8.663091	1.967550783185259
Sr	87	38	4.2249	4.2549	8.705236	8.659752	1.965744088591193
Sr	88	38	4.2240	4.2695	8.732595	8.656290	1.963966976339631
Y	89	39	4.2430	4.2840	8.713978	8.652708	1.962218628021685
Zr	90	40	4.2694	4.2984	8.709969	8.649010	1.960498256851153
Zr	91	40	4.2845	4.3127	8.693314	8.645198	1.958805106104303
Zr	92	40	4.3057	4.3269	8.692678	8.641275	1.957138447652745
Mo	92	42	4.3151	4.3269	8.657730	8.641275	1.957138447652745
Nb	93	41	4.3240	4.3410	8.664184	8.637246	1.955497580583371
Zr	94	40	4.3320	4.3550	8.666801	8.633112	1.953881829898621
Mo	94	42	4.3529	4.3550	8.662333	8.633112	1.953881829898621
Mo	95	42	4.3628	4.3690	8.648720	8.628876	1.952290545292565
Mo	96	42	4.3847	4.3828	8.653987	8.624541	1.950723099996405
Ru	96	44	4.3908	4.3828	8.609412	8.624541	1.950723099996405
Mo	97	42	4.3880	4.3966	8.635092	8.620109	1.949178889690030
Mo	98	42	4.4091	4.4102	8.635168	8.615583	1.947657331474187
Ru	98	44	4.4229	4.4102	8.62031	8.61558	1.947657331474187
Ru	99	44	4.4338	4.4238	8.608712	8.610965	1.946157862899922
Ru	100	44	4.4531	4.4373	8.619359	8.606258	1.944679941051426
Ru	101	44	4.4606	4.4507	8.601365	8.601463	1.943223041678503
Ru	102	44	4.4809	4.4640	8.607427	8.596583	1.941786658376123
Pd	102	46	4.4827	4.4640	8.580290	8.596583	1.941786658376123
Rh	103	45	4.4945	4.4772	8.584192	8.591620	1.940370301807507
Pd	104	46	4.5078	4.4904	8.584848	8.586576	1.938973498968275

Continued on next page

Table 2 – *Continued from previous page*

Name	A	Z	$R^{\text{exp.}}$	$R^{\text{num.}}$	$E_B^{\text{exp.}}$	$E_B^{\text{num.}}$	γ
Ru	104	44	4.5098	4.4904	8.587399	8.586576	1.938973498968275
Pd	105	46	4.5150	4.5035	8.570650	8.581453	1.937595792489287
Pd	106	46	4.5318	4.5165	8.579992	8.576252	1.936236739975294
Cd	106	48	4.5383	4.5165	8.539048	8.576252	1.936236739975294
Ag	107	47	4.5454	4.5294	8.553900	8.570976	1.934895913377873
Cd	108	48	4.5577	4.5422	8.550019	8.565626	1.933572898399922
Pd	108	46	4.5563	4.5422	8.567023	8.565626	1.933572898399922
Ag	109	47	4.5638	4.5550	8.547915	8.560203	1.932267293930503
Pd	110	46	4.5782	4.5677	8.547162	8.554710	1.930978711507522
Cd	110	48	4.5765	4.5677	8.551275	8.554710	1.930978711507522
Cd	111	48	4.5845	4.5804	8.537079	8.549149	1.929706774807386
Cd	112	48	4.5944	4.5929	8.544730	8.543519	1.928451119159275
Sn	112	50	4.5948	4.5929	8.513618	8.543519	1.928451119159275
In	113	49	4.6010	4.6054	8.522929	8.537824	1.927211391083395
Sn	114	50	4.6099	4.6178	8.522566	8.532064	1.925987247851143
Cd	114	48	4.6087	4.6178	8.531513	8.532064	1.925987247851143
Sn	115	50	4.6148	4.6302	8.514069	8.526241	1.924778357066431
Sn	116	50	4.6250	4.6425	8.523116	8.520357	1.923584396266858
Sn	117	50	4.6302	4.6547	8.509611	8.514412	1.922405052543427
Sn	118	50	4.6393	4.6668	8.516533	8.508407	1.921240022178119
Sn	119	50	4.6438	4.6789	8.499449	8.502345	1.920089010298075
Sn	120	50	4.6519	4.6909	8.504492	8.496226	1.918951730545584
Te	120	52	4.7038	4.6909	8.477034	8.496226	1.918951730545584
Sb	121	51	4.6802	4.7029	8.482066	8.490052	1.917827904763047
Te	122	52	4.7095	4.7148	8.478140	8.483823	1.916717262692254
Sn	122	50	4.6634	4.7148	8.487907	8.483823	1.916717262692254
Sb	123	51	4.6879	4.7266	8.472328	8.477540	1.915619541686807
Te	123	52	4.7117	4.7266	8.465546	8.477540	1.915619541686807
Te	124	52	4.7183	4.7384	8.473279	8.471206	1.914534486437504
Xe	124	54	4.7661	4.7384	8.437565	8.471206	1.914534486437504
Sn	124	50	4.6735	4.7384	8.467421	8.471206	1.914534486437504
Te	125	52	4.7204	4.7501	8.458045	8.464820	1.913461848709503
Te	126	52	4.7266	4.7618	8.463248	8.458383	1.912401387091375
Xe	126	54	4.7722	4.7618	8.443541	8.458383	1.912401387091375
I	127	53	4.7500	4.7734	8.445487	8.451898	1.911352866754402
Xe	128	54	4.7774	4.7850	8.443298	8.445364	1.910316059222751
Xe	129	54	4.7775	4.7964	8.431390	8.438783	1.909290742152922
Ba	130	56	4.8283	4.8079	8.405549	8.432156	1.908276699122978
Xe	130	54	4.7818	4.8079	8.437731	8.432156	1.908276699122978
Xe	131	54	4.7808	4.8193	8.423736	8.425482	1.907273719430179
Xe	132	54	4.7859	4.8306	8.427622	8.418764	1.906281597897336

Continued on next page

Table 2 – *Continued from previous page*

Name	A	Z	$R^{\text{exp.}}$	$R^{\text{num.}}$	$E_B^{\text{exp.}}$	$E_B^{\text{num.}}$	γ
Ba	132	56	4.8303	4.8306	8.409375	8.418764	1.906281597897336
Cs	133	55	4.8041	4.8418	8.409978	8.412003	1.905300134686859
Xe	134	54	4.7899	4.8531	8.413699	8.405198	1.904329135122647
Ba	134	56	4.8322	4.8531	8.408171	8.405198	1.904329135122647
Ba	135	56	4.8294	4.8642	8.397533	8.398350	1.903368409519181
Ce	136	58	4.8739	4.8753	8.373760	8.391462	1.902417773017244
Ba	136	56	4.8334	4.8753	8.402755	8.391462	1.902417773017244
Ba	137	56	4.8314	4.8864	8.391827	8.384532	1.901477045426730
Ba	138	56	4.8378	4.8974	8.393420	8.377562	1.900546051075015
Ce	138	58	4.8737	4.8974	8.37708	8.37756	1.900546051075015
La	139	57	4.8550	4.9084	8.378025	8.370554	1.899624618661961
Ce	140	58	4.8771	4.9193	8.376317	8.363506	1.898712581120185
Pr	141	59	4.8919	4.9301	8.353992	8.356420	1.897809775480838
Ce	142	58	4.9063	4.9410	8.347071	8.349298	1.896916042744723
Nd	142	60	4.9123	4.9410	8.346030	8.349298	1.896916042744723
Nd	143	60	4.9254	4.9517	8.330488	8.342138	1.896031227758121
Sm	144	62	4.9524	4.9624	8.303679	8.334943	1.895155179093460
Nd	145	60	4.9535	4.9731	8.309187	8.327712	1.894287748934647
Nd	146	60	4.9696	4.9837	8.304092	8.320446	1.893428792966205
Nd	148	60	4.9999	5.0048	8.277177	8.305813	1.891735743208532
Sm	149	62	5.0134	5.0153	8.263466	8.298446	1.890901377354422
Sm	150	62	5.0387	5.0258	8.261621	8.291047	1.890074941367280
Sm	152	62	5.0819	5.0465	8.244061	8.276153	1.888445348587004
Eu	153	63	5.1115	5.0568	8.228699	8.268659	1.887641943800672
Sm	154	62	5.1053	5.0671	8.226835	8.261135	1.886845972727570
Gb	154	64	5.1223	5.0671	8.224796	8.261135	1.886845972727570
Gb	155	64	5.1319	5.0773	8.213251	8.253581	1.886057318209837
Dy	156	66	5.1622	5.0875	8.192433	8.245997	1.885275865684704
Gb	156	64	5.1420	5.0875	8.215322	8.245997	1.885275865684704
Gb	157	64	5.1449	5.0977	8.203504	8.238385	1.884501503110640
Gb	158	64	5.1569	5.1078	8.201819	8.230743	1.883734120896110
Dy	158	66	5.1815	5.1078	8.190130	8.230743	1.883734120896110
Tb	159	65	5.0600	5.1178	8.188800	8.223074	1.882973611830810
Dy	160	66	5.1951	5.1279	8.184054	8.215377	1.882219871019077
Gd	160	64	5.1734	5.1279	8.183014	8.215377	1.882219871019077
Dy	161	66	5.1962	5.1379	8.173310	8.207652	1.881472795815909
Er	162	68	5.2246	5.1478	8.152397	8.199901	1.880732285764774
Dy	162	66	5.2074	5.1478	8.173457	8.199901	1.880732285764774
Dy	163	66	5.2099	5.1577	8.161785	8.192123	1.879998242537775
Dy	164	66	5.2218	5.1676	8.158714	8.184320	1.879270569877631
Er	164	68	5.2389	5.1676	8.149020	8.184320	1.879270569877631

Continued on next page

Table 2 – *Continued from previous page*

Name	A	Z	$R^{\text{exp.}}$	$R^{\text{num.}}$	$E_B^{\text{exp.}}$	$E_B^{\text{num.}}$	γ
Ho	165	67	5.2022	5.1774	8.146964	8.176490	1.878549173541836
Er	166	68	5.2516	5.1872	8.141959	8.168635	1.877833961248146
Er	167	68	5.2560	5.1970	8.131746	8.160756	1.877124842622655
Er	168	68	5.2644	5.2067	8.129601	8.152852	1.876421729148642
Yb	168	70	5.2702	5.2067	8.111898	8.152852	1.876421729148642
Tm	169	69	5.2256	5.2164	8.114473	8.144923	1.875724534117927
Er	170	68	5.2789	5.2260	8.111959	8.136971	1.875033172583114
Yb	170	70	5.2853	5.2260	8.106609	8.136971	1.875033172583114
Yb	171	70	5.2906	5.2356	8.097882	8.128995	1.874347561311723
Yb	172	70	5.2995	5.2452	8.097429	8.120996	1.873667618741784
Yb	173	70	5.3046	5.2547	8.087427	8.112975	1.872993264938715
Yb	174	70	5.3108	5.2642	8.083847	8.104930	1.872324421553529
Lu	175	71	5.3700	5.2737	8.069140	8.096864	1.871661011782399
Hf	176	72	5.3286	5.2831	8.061359	8.088776	1.871002960327636
Yb	176	70	5.3215	5.2831	8.064085	8.088776	1.871002960327636
Hf	177	72	5.3309	5.2925	8.051835	8.080666	1.870350193359751
Hf	178	72	5.3371	5.3019	8.049442	8.072535	1.869702638480259
Hf	179	72	5.3408	5.3113	8.038546	8.064383	1.869060224686682
Hf	180	72	5.3470	5.3206	8.034930	8.056210	1.868422882337254
Ta	181	73	5.3507	5.3298	8.023400	8.048017	1.867790543118027
W	182	74	5.3559	5.3391	8.018308	8.039804	1.867163140009889
W	183	74	5.3611	5.3483	8.008322	8.031571	1.866540607257118
W	184	74	5.3658	5.3574	8.005077	8.023318	1.865922880336927
Os	184	76	5.3823	5.3574	7.988677	8.023318	1.865922880336927
Re	185	75	5.3596	5.3666	7.991009	8.015046	1.865309895929486
W	186	74	5.3743	5.3757	7.988601	8.006755	1.864701591889463
Os	187	76	5.3933	5.3848	7.973780	7.998445	1.864097907217535
Os	188	76	5.3993	5.3938	7.973864	7.990117	1.863498782033505
Os	189	76	5.4016	5.4028	7.963002	7.981770	1.862904157549983
Os	190	76	5.4062	5.4118	7.962104	7.973405	1.862313976046459
Ir	191	77	5.3968	5.4208	7.948113	7.965023	1.861728180844594
Os	192	76	5.4126	5.4297	7.948525	7.956622	1.861146716284074
Pt	192	78	5.4169	5.4297	7.942491	7.956622	1.861146716284074
Ir	193	77	5.4032	5.4386	7.938133	7.948205	1.860569527698860
Pt	194	78	5.4236	5.4475	7.935941	7.939770	1.859996561394610
Pt	195	78	5.4270	5.4563	7.926552	7.931318	1.859427764626352
Pt	196	78	5.4307	5.4651	7.926529	7.922849	1.858863085576737
Hg	196	80	5.4385	5.4651	7.914369	7.922849	1.858863085576737
Au	197	79	5.4371	5.4739	7.915654	7.914364	1.858302473335395
Pt	198	78	5.4383	5.4827	7.914150	7.905863	1.857745877878276
Hg	198	80	5.4463	5.4827	7.911552	7.905863	1.857745877878276

Continued on next page

Table 2 – *Continued from previous page*

Name	A	Z	$R^{\text{exp.}}$	$R^{\text{num.}}$	$E_B^{\text{exp.}}$	$E_B^{\text{num.}}$	γ
Hg	199	80	5.4474	5.4914	7.905279	7.897345	1.857193250047730
Hg	200	80	5.4551	5.5001	7.905895	7.888812	1.856644541533518
Hg	201	80	5.4581	5.5088	7.897560	7.880263	1.856099704853727
Hg	202	80	5.4648	5.5174	7.896850	7.871698	1.855558693336665
Tl	203	81	5.4666	5.5260	7.886053	7.863118	1.855021461102933
Hg	204	80	5.4744	5.5346	7.885545	7.854523	1.854487963048309
Pb	204	82	5.4803	5.5346	7.879932	7.854523	1.854487963048309
Tl	205	81	5.4759	5.5432	7.878394	7.845912	1.853958154826700
Pb	206	82	5.4902	5.5517	7.875362	7.837287	1.853431992833947
Pb	207	82	5.4943	5.5602	7.869866	7.828648	1.852909434191629
Pb	208	82	5.5012	5.5687	7.867453	7.819994	1.852390436731829
Bi	209	83	5.5211	5.5772	7.847987	7.811325	1.851874958981518
Ra	226	88	5.7211	5.7172	7.661962	7.661932	1.843613253087140
Th	229	90	5.7557	5.7412	7.634650	7.635200	1.842246251422184
Th	230	90	5.7670	5.7491	7.630996	7.626267	1.841796196593272
Th	232	90	5.7848	5.7650	7.615033	7.608367	1.840904328898081
U	233	92	5.8203	5.7729	7.603956	7.599401	1.840462458679807
U	234	92	5.8291	5.7807	7.600715	7.590424	1.840023260016007
U	235	92	5.8337	5.7886	7.590914	7.581436	1.839586705273448
U	236	92	5.8431	5.7964	7.586484	7.572438	1.839152767221810
U	238	92	5.8571	5.8120	7.570125	7.554410	1.838292634239833
Pu	239	94	5.8601	5.8198	7.560318	7.545380	1.837866386796573
Pu	240	94	5.8701	5.8275	7.556042	7.536341	1.837442651004169

References

- [1] Bruce R. Barrett, Petr Navratil, and James P. Vary. Ab initio no core shell model. *Prog. Part. Nucl. Phys.*, 69:131–181, 2013.
- [2] I. Stetcu and J. Rotureau. Effective interactions and operators in no-core shell model. *Prog. Part. Nucl. Phys.*, 69:182–224, 2013.
- [3] S. K. Bogner, R. J. Furnstahl, and A. Schwenk. From low-momentum interactions to nuclear structure. *Prog. Part. Nucl. Phys.*, 65:94–147, 2010.
- [4] Steven Weinberg. Phenomenological Lagrangians. *Physica A*, 96(1-2):327–340, 1979.
- [5] C. Ordonez and U. van Kolck. Chiral lagrangians and nuclear forces. *Phys. Lett. B*, 291:459–464, 1992.
- [6] H. W. Hammer, S. König, and U. van Kolck. Nuclear effective field theory: status and perspectives. *Rev. Mod. Phys.*, 92(2):025004, 2020.

- [7] Gerard 't Hooft. A Planar Diagram Theory for Strong Interactions. *Nucl. Phys. B*, 72:461, 1974.
- [8] Edward Witten. Global Aspects of Current Algebra. *Nucl. Phys. B*, 223:422–432, 1983.
- [9] Edward Witten. Current Algebra, Baryons, and Quark Confinement. *Nucl. Phys. B*, 223:433–444, 1983.
- [10] Gregory S. Adkins, Chiara R. Nappi, and Edward Witten. Static Properties of Nucleons in the Skyrme Model. *Nucl. Phys. B*, 228:552, 1983.
- [11] T. H. R. Skyrme. A Nonlinear field theory. *Proc. Roy. Soc. Lond. A*, 260:127–138, 1961.
- [12] T. H. R. Skyrme. A Unified Field Theory of Mesons and Baryons. *Nucl. Phys.*, 31:556–569, 1962.
- [13] Richard A. Battye and Paul M. Sutcliffe. Symmetric skyrmions. *Phys. Rev. Lett.*, 79:363–366, 1997.
- [14] Richard A. Battye and Paul M. Sutcliffe. Solitonic fullerene structures in light nuclei. *Phys. Rev. Lett.*, 86:3989–3992, 2001.
- [15] N. S. Manton and P. Sutcliffe. *Topological solitons*. Cambridge Monographs on Mathematical Physics. Cambridge University Press, 2004.
- [16] N. S. Manton and P. J. Ruback. Skyrmions in Flat Space and Curved Space. *Phys. Lett. B*, 181:137–140, 1986.
- [17] Derek Harland. Topological energy bounds for the Skyrme and Faddeev models with massive pions. *Phys. Lett. B*, 728:518–523, 2014.
- [18] Paul Sutcliffe. Skyrmions, instantons and holography. *JHEP*, 08:019, 2010.
- [19] Carlos Naya and Paul Sutcliffe. Skyrmions in models with pions and rho mesons. *JHEP*, 05:174, 2018.
- [20] Carlos Naya and Paul Sutcliffe. Skyrmions and clustering in light nuclei. *Phys. Rev. Lett.*, 121(23):232002, 2018.
- [21] C. Adam, J. Sanchez-Guillen, and A. Wereszczynski. A Skyrme-type proposal for baryonic matter. *Phys. Lett. B*, 691:105–110, 2010.
- [22] C. Adam, J. Sanchez-Guillen, and A. Wereszczynski. A BPS Skyrme model and baryons at large N_c . *Phys. Rev. D*, 82:085015, 2010.
- [23] C. Adam, C. Naya, J. Sanchez-Guillen, and A. Wereszczynski. Bogomol’nyi-Prasad-Sommerfield Skyrme Model and Nuclear Binding Energies. *Phys. Rev. Lett.*, 111(23):232501, 2013.

- [24] C. Adam, C. Naya, J. Sanchez-Guillen, R. Vazquez, and A. Wereszczynski. BPS Skyrmions as neutron stars. *Phys. Lett. B*, 742:136–142, 2015.
- [25] I. Zahed and G. E. Brown. The Skyrme Model. *Phys. Rept.*, 142:1–102, 1986.
- [26] V. G. Makhankov, Y. P. Rybakov, and V. I. Sanyuk. *The Skyrme model: Fundamentals, methods, applications*. 1993.
- [27] Olga V. Manko, Nicholas S. Manton, and Stephen W. Wood. Light nuclei as quantized skyrmions. *Phys. Rev. C*, 76:055203, 2007.
- [28] Richard A. Battye, Nicholas S. Manton, Paul M. Sutcliffe, and Stephen W. Wood. Light Nuclei of Even Mass Number in the Skyrme Model. *Phys. Rev. C*, 80:034323, 2009.
- [29] C. J. Halcrow, C. King, and N. S. Manton. Oxygen-16 Spectrum from Tetrahedral Vibrations and their Rotational Excitations. *Int. J. Mod. Phys. E*, 28(04):1950026, 2019.
- [30] C. J. Halcrow and J. I. Rawlinson. Electromagnetic transition rates of ^{12}C and ^{16}O in rotational-vibrational models. *Phys. Rev. C*, 102(1):014314, 2020.
- [31] Chris Halcrow and Derek Harland. An attractive spin-orbit potential from the Skyrme model. *Phys. Rev. Lett.*, 125(4):042501, 2020.
- [32] L. A. Ferreira. Exact self-duality in a modified Skyrme model. *JHEP*, 07:039, 2017.
- [33] I. Angeli and K. P. Marinova. Table of experimental nuclear ground state charge radii: An update. *Atom. Data Nucl. Data Tabl.*, 99(1):69–95, 2013.
- [34] Meng Wang, G. Audi, F.G. Kondev, W. J. Huang, S. Naimi, and Xing Xu. The Ame2016 atomic mass evaluation, (II) Tables, graphs and references. *Chin. Phys. C*, 41(3):030003, 2017.
- [35] G. Audi, F. G. Kondev, Meng Wang, W. J. Huang, and S. Naimi. The NUBASE2016 evaluation of nuclear properties. *Chin. Phys. C*, 41(3):030001, 2017.
- [36] L. A. Ferreira and L. R. Livramento. Self-Duality in the Context of the Skyrme Model. *JHEP*, 09:031, 2020.
- [37] Sidney R. Coleman. The Fate of the False Vacuum. 1. Semiclassical Theory. *Phys. Rev. D*, 15:2929–2936, 1977. [Erratum: Coleman,S., Phys.Rev.D 16, 1248 (1977)].
- [38] Sidney R. Coleman, V. Glaser, and Andre Martin. Action Minima Among Solutions to a Class of Euclidean Scalar Field Equations. *Commun. Math. Phys.*, 58:211–221, 1978.
- [39] C. Adam, L. A. Ferreira, E. da Hora, A. Wereszczynski, and W. J. Zakrzewski. Some aspects of self-duality and generalised BPS theories. *JHEP*, 08:062, 2013.
- [40] L. A. Ferreira and Wojtek J. Zakrzewski. A Skyrme-like model with an exact BPS bound. *JHEP*, 09:097, 2013.

- [41] L. A. Ferreira and Ya. Shnir. Exact Self-Dual Skyrmons. *Phys. Lett. B*, 772:621–627, 2017.
- [42] G. H. Derrick. Comments on nonlinear wave equations as models for elementary particles. *J. Math. Phys.*, 5:1252–1254, 1964.
- [43] D. Adhikari *et al.* [PREX], Accurate Determination of the Neutron Skin Thickness of ^{208}Pb through Parity-Violation in Electron Scattering, *Phys. Rev. Lett.* **126** (2021) no.17, 172502.